Cell cycle S-phase arrest drives cell extrusion

Vivek K. Dwivedi[α], Carlos Pardo-Pastor[†], Rita Droste[α], Daniel P. Denning[#,α], Jody Rosenblatt[†], and H. Robert Horvitz[α,*]

[α]Howard Hughes Medical Institute, Department of Biology, Massachusetts Institute of Technology, Cambridge, MA 02139, USA

[†]Randall Division of Cell and Molecular Biophysics, King's College London, London SE1 1UL, UK

[#]Novartis Institutes for BioMedical Research, Cambridge, MA 02139

*Correspondence: horvitz@mit.edu

SUMMARY

Cell extrusion is a process of cell elimination in which a cell is squeezed out from its tissue of origin. Extrusion occurs in organisms as diverse as sponges, nematodes, insects, fish and mammals. Defective extrusion is linked to many epithelial disorders, including cancer. Despite broad occurrence, cell-intrinsic triggers of extrusion conserved across phyla are generally unknown. We combined genome-wide genetic screens with live-imaging studies of *C. elegans* embryos and mammalian epithelial cultures and found that S-phase arrest induced extrusion in both. Cells extruded from *C. elegans* embryos exhibited S-phase arrest, and RNAi treatments that specifically prevent S-phase entry or arrest blocked cell extrusion. Pharmacological induction of S-phase arrest was sufficient to promote cell extrusion from a canine epithelial monolayer. Thus, we have discovered an evolutionarily conserved cell-cycle-dependent trigger of cell extrusion. We suggest that S-phase-arrest induced cell extrusion plays a key role in physiology and disease.

INTRODUCTION

During development and homeostasis, cells are eliminated by a variety of mechanisms. One such mechanism is cell extrusion, in which a cell is expelled from a layer of cells while the continuity of the layer is maintained. Cell extrusion has been observed in and studied using a wide variety of organisms, including the sponge *H. caerulea*, *C. elegans*, *D. melanogaster*, zebrafish and mammals, suggesting that cell extrusion is an evolutionarily conserved mechanism of eliminating unnecessary or harmful cells (De Goeij *et al*., 2009; reviewed by Gudipaty and Rosenblatt, 2017 and Ohsawa *et al*., 2018). Vertebrate epithelial tissues use cell extrusion as the primary mode of cell elimination (Gu and Rosenblatt, 2012; Günther and Seyfert, 2018). Cell extrusion plays a key role in epithelial defense mechanisms that remove oncogene-transformed cells from epithelial layers (reviewed by Kajita and Fujita, 2015). Excessive cell extrusion can produce epithelial layer breaches, like those observed in asthma and Crohn's disease (Gudipaty and Rosenblatt, 2017). Decreased cell extrusion leads to the formation of epithelial cell masses and confers resistance to cell death (Eisenhoffer *et al*., 2012; Gu *et al*., 2015). Intestinal polyps, which can develop into colon cancers, lack clearly identifiable cell extrusions (Eisenhoffer *et al*., 2012), suggesting that extrusion might be important for the prevention of polyps and intestinal cancers. Disruption and subversion of the cell-extrusion process likely promotes tumor growth and metastasis in pancreatic, lung and colon cancer (Gu *et al.*, 2015).

While several mechanisms of cell extrusion have been described for *Drosophila* and vertebrates, these mechanisms have focused on the cell-cell interactions and cellular contexts, such as crowding, topological defects, cell competition, etc., that induce cell extrusion (reviewed by Fadul and Rosenblatt, 2018, Ohsawa *et al*., 2018). A cell-intrinsic trigger that can induce extrusion in organisms of different phyla has not been identified.

C. elegans is an excellent organism for the study of evolutionarily conserved mechanisms of cell elimination. The discovery of a conserved set of genes regulating caspase-mediated apoptosis in *C. elegans* has been fundamental to the understanding of programmed cell death in metazoa (reviewed by Fuchs and Steller, 2011). Cell extrusion can eliminate cells fated for death in *C. elegans* (Denning *et al*., 2012). Embryos with mutations in the caspase-mediated apoptosis pathway, e.g. loss-of-function mutants of the caspase gene *ced-3*, eliminate by extrusion a subset of cells that are otherwise eliminated by caspase-mediated apoptosis and engulfment in wild-type embryos. Denning *et al*. (2012) determined that the PAR-4 – PIG-1 (mammalian homologs LKB1 – MELK) kinase cascade is required for cell extrusion by *C. elegans ced-3(lf)* embryos. However, LKB1 (mammalian homolog of PAR-4) was found to prevent extrusion from mouse embryos (Krawchuk *et al*., 2015), indicating that LKB1/PAR-4 is likely not a driver but a regulator of cell extrusion in nematodes and mammals. No “caspase-equivalent” cell-intrinsic driver of cell extrusion is known.

To seek a conserved cell-intrinsic driver of extrusion, we first comprehensively identified genes and pathways that control cell extrusion by *C. elegans* and then tested the corresponding pathways for a role in mammalian cell extrusion. Briefly, we performed a genome-wide RNAi screen for defective cell extrusion by *C. elegans* and used confocal microscopy to analyze the effect of RNAi against the identified genes on the cell extrusion process. From this analysis, we found that cell extrusion by *C. elegans* requires cell-autonomous cell cycle entry and subsequent S-phase arrest and that circumventing S-phase arrest blocks extrusion. We then tested and confirmed that pharmacological induction of S-phase arrest with hydroxyurea (HU) (Timson, 1975; Bianchi *et al*., 1983) promotes cell extrusion of mammalian epithelial cells. We conclude that S-phase arrest is a conserved cell-intrinsic trigger of cell extrusion in *C. elegans* and mammals.

RESULTS

Genome-wide RNAi screen identified cell-cycle genes as candidate regulators of cell extrusion

In wild-type *C. elegans* embryos, 131 cells are eliminated by caspase-mediated apoptosis and engulfment. By contrast, in *C. elegans ced-3* caspase mutants, a few of the cells that would normally undergo programmed cell death instead are extruded from the developing embryo (Denning *et al*., 2012). Of the approximately six cells extruded from *ced-3(lf)* embryos, the cell ABplpappap is most frequently extruded (Denning *et al*., 2012 and unpublished). If extrusion fails to occur, ABplpappap (or descendants of ABplpappap) survive(s) and

113 differentiate(s) into one (or two) supernumerary excretory cell(s), producing
114 mutant animals with the two (or three)-excretory-cell (Tex) phenotype; by
115 contrast both wild-type and *ced-3(lf)* animals have one excretory cell (Denning *et*
116 *al*., 2012; Figure 1A). Mutations that reduce ABplpappap extrusion and produce
117 the Tex phenotype also reduce the extrusion of other cells (Denning *et al*., 2012),
118 making the Tex phenotype a convenient marker for defective cell extrusion.
119 We performed a genome-wide RNAi screen for the Tex phenotype in *ced-*
120 *3(lf)* animals expressing the GFP excretory-cell reporter $P_{pgp\text{-}12}$*::4xNLS::GFP*
121 (Figure 1B; Denning *et al*., 2012). We screened 11,511 RNAi clones (targeting
122 about 55% of the ~20,000 *C. elegans* genes by feeding (Rual *et al*., 2004)) and
123 found 30 clones targeting 27 unique genes that consistently produced a Tex
124 phenotype. Three RNAi clones identified genes previously reported to function in
125 cell extrusion, *grp-1*, *arf-1.2* and *arf-3* (Denning *et al*., 2012), confirming that this
126 RNAi screen could identify cell extrusion mutants. Unexpectedly, 10 of the RNAi
127 clones targeted genes that control cell-cycle progression (Figure 1C), suggesting
128 a possible role for the cell cycle in controlling cell extrusion.
129 We then tested a nearly complete set of *C. elegans* cell cycle genes for
130 functional roles in cell extrusion (van den Heuvel, 2005) using an RNAi library of
131 61 publically available and, when necessary, newly generated clones with each
132 clone targeting a unique gene (Kamath *et al*., 2003; Rual *et al*., 2004; Materials
133 and Methods). We found that RNAi against four additional cell cycle genes
134 produced a Tex phenotype (Figure 1C, Supplemental Table 1).

Most of the 14 cell-cycle genes we identified are well-characterized regulators of S-phase entry and progression. These genes include *cdc-25.2*, which encodes a homolog of the CDK-activating phosphatase CDC25 (Lee *et al*., 2016); *cdk-1* and *cdk-2*, which encode homologs of CDK1 and CDK2, respectively (Boxem, 2006); *cye-1* and *cya-1*, which encode homologs of S-phase cyclins E and A, respectively (Fay and Han, 2000; Kreutzer *et al*., 1995); and *psf-1*, *psf-2* and *psf-3*, which encode homologs of pre-replicative and replicative complex components PSF1, PSF2 and PSF3, respectively (Ossareh-Nazari *et al*., 2016; Figure 1C). All of these cell cycle genes with S-phase function are required for *C. elegans* viability. However, it is unlikely that a general reduction in embryonic fitness causes the Tex phenotype, as RNAi against essential genes involved in other phases of the cell cycle (e.g., metaphase-to-anaphase transition genes *mat-1*, *mat-2*, etc. (reviewed by Yeong, 2004)) or those involved in transcription (e.g., *cdk-7* and *cdk-9* (Wallenfang and Seydoux, 2002; Bowman *et al*., 2013)) did not produce the Tex phenotype despite producing extensive lethality (Supplemental Table 1). Furthermore, as with RNAi targeting *pig-1* or other genes generally required for cell extrusion (Denning *et al*., 2012), RNAi against 13 of the 14 identified cell cycle genes produced the Tex phenotype in *ced-3(lf)* mutants but not in wild-type animals (Supplemental Table 2). Altogether, we found that defects in S-phase entry and progression are specifically associated with a synthetic *ced-3*-dependent Tex phenotype, suggesting a role for these cell-cycle genes in promoting cell extrusion.

S-phase entry genes function to promote cell extrusion

158 Whereas defects in the extrusion of ABplpappap cause the Tex
159 phenotype, it is possible that the supernumerary excretory cell(s) of some
160 mutants could arise from other cell lineages. To directly determine whether
161 genes functioning in S-phase entry are important for cell extrusion, we used time-
162 lapse confocal microscopy to monitor the extrusion of ABplpappap from *ced-3(lf)*
163 embryos deficient in *cye-1* or *cdk-2*. To assess extrusion events, we imaged live
164 embryos with ABplpappap in focus over a 50-minute period ending at the
165 completion of ventral enclosure, when epidermal cells meet at the ventral midline
166 following a dorsolateral migration; ventral enclosure coincides with the cell
167 extrusion that occurs in *ced-3(lf)* embryos (Denning *et al*., 2012). For clarity, we
168 refer below to embryos from *ced-3(lf)* parents treated with RNAi against a gene,
169 say *gene-x*, as "*gene-x(RNAi)* embryos" and to embryos from *ced-3(lf)* parents
170 treated with RNAi against the empty vector as "control embryos."

171 In control embryos, cells neighboring ABplpappap on the ventral surface
172 gradually disappeared from view until ABplpappap was left completely isolated
173 (Figure 2A, Movie 1), indicating that ABplpappap had been extruded from the
174 embryo. By comparison, in *cye-1(RNAi)* embryos (Figure 2B, Movie 2) or *cdk-*
175 *2(RNAi)* embryos (Figure 2C, Movie 3), ABplpappap was surrounded by cells
176 throughout the imaging period and hence remained within the embryo, failing to
177 detach. Using dorso-ventral confocal sections from the live embryo imaging, we
178 reconstructed sagittal views of the embryos during ventral enclosure. These
179 views confirmed that ABplpappap was extruded ventrally from 10 of 11 control
180 embryos (Figure 2D, Supplemental Figure 1), whereas ABplpappap failed to

detach and was incorporated into the body of *cye-1(RNAi)* embryos (11 of 11 embryos; Figure 2E, Supplemental Figure 2) or *cdk-2(RNAi)* embryos (10 of 11 embryos; Figure 2F, Supplemental Figure 3). These findings demonstrate that the S-phase entry genes *cye-1* and *cdk-2* are required for ABplpappap extrusion in *ced-3* embryos.

Entry into S phase is required for and precedes cell extrusion

Since genes that promote S-phase entry are required for ABplpappap extrusion, we tested if cells that undergo extrusion enter S phase. We used a previously characterized reporter transgene that expresses a truncated human DNA Helicase B (tDHB)-GFP fusion protein optimized for expression in *C. elegans* and that changes its intracellular location in response to CDK1 and CDK2 activity (van Rijnberk *et al*., 2017; Spencer *et al*., 2013). tDHB-GFP is enriched in the nuclei of quiescent or post-mitotic cells, whereas it exhibits an increasing cytoplasmic bias as cells progress from S-phase through mitosis (Figure 3A; Spencer *et al*., 2013). In control embryos, tDHB-GFP was mostly absent from the ABplpappap nucleus (10 of 10 embryos) both before ventral enclosure (Figure 3B) and as it was extruded (Figure 3E), indicating that ABplpappap entered S phase prior to its extrusion during the period of ventral enclosure. Cells extruded from other sites of the embryo also displayed low levels of nuclear tDHB-GFP (Figures 3I-L). By contrast, in *cye-1(RNAi)* embryos (Figures 3C, 3F) or *cdk-2(RNAi)* embryos (Figures 3D, 3G) the ABplpappap nucleus scored positive for the tDHB-GFP fusion protein during the period around ventral enclosure (10 of 10 embryos each for each RNAi treatment),

suggesting that RNAi against these genes prevented both the entry of ABplpappap into S-phase and its extrusion. Quantification of the nuclear-to-cytoplasmic ratio of tDHB-GFP fluorescence intensity in ABplpappap in control, *cye-1(RNAi)* and *cdk-2(RNAi)* embryos at varying stages with respect to ventral enclosure confirmed these observations (Figure 3H). Some cells were still extruded in *cye-1(RNAi)* and *cdk-2(RNAi)* embryos, likely reflecting incomplete inhibition of gene function by RNAi. Consistently, such cells displayed low levels of nuclear tDHB-GFP, indicating that those cells entered the cell cycle (Supplemental Figure 4). Thus, cell-cycle entry appears to be a functionally critical step in the process of cell extrusion.

To define more precisely the cell-cycle phase that facilitates cell extrusion, we used a second reporter transgene (GFP::PCN-1), which expresses an N-terminal translational fusion of GFP to the *C. elegans* homolog of the DNA replication processivity factor PCNA (Brauchle *et al*., 2003). PCNA in mammalian cells and early *C. elegans* embryonic cells exhibits a punctate, sub-nuclear localization only during S-phase (Figure 4A; Brauchle *et al*., 2003; Zerjatke *et al*., 2017). The localization pattern of GFP::PCN-1 in cell cycles of cells close to ABplpappap on the embryonic ventral surface matched that described for early embryonic cells and contrasted with the continuous accumulation of GFP::PCN-1 observed during the *C. elegans* germline cell cycle (Supplemental Figure 5; Movie 4; Brauchle *et al*., 2003; Kocsisova *et al*., 2018). We found that in control embryos GFP::PCN-1 was localized in bright sub-nuclear foci in ABplpappap immediately prior to the initiation of ventral enclosure, indicating that this cell was

in S phase (5 of 5 embryos) (Figure 4B). By contrast, ABplpappap showed a diffuse nuclear localization of GFP::PCN-1 in *cye-1(RNAi)* (Figure 4C, 4F) and *cdk-2(RNAi)* (Figure 4D, 4G) embryos, both before (5 of 5 embryos each) and after ventral enclosure (5 of 5 embryos each), indicating a failure to enter the cell cycle. We conclude that cells to be extruded must enter S phase for extrusion to occur and that blocking S-phase entry prevents cell extrusion.

Extruding cells exhibit an arrested S phase and experience replication stress

Given that cells required cell-cycle entry for extrusion, we examined the extent of cell-cycle progression in these cells as they were extruded. In control embryos, we found that GFP::PCN-1 was localized in bright sub-nuclear foci in ABplpappap both before (5 of 5 embryos) and after extrusion (5 of 5 embryos) (Figure 4B, 4E), indicating that ABplpappap entered but did not exit S phase. We observed no significant changes of GFP::PCN-1 localization in ABplpappap up to and after its extrusion over a period of 35 min (Figure 4H), indicating that it remained arrested in S phase. A second unidentified extruding cell showed a similarly unchanging GFP::PCN-1 localization pattern (Figure 4H). To determine if the S-phase arrest observed in ABplpappap and the other extruding cell is a general feature of cell extrusion, we examined other extruded cells in the embryo. Nearly all cells extruded by *ced-3(lf)* embryos displayed bright sub-nuclear foci of GFP::PCN-1, consistent with an arrested S phase in these cells (Figures 4H-J).

Arrest of DNA replication during S phase can occur as a result of replication stress, which can arise for many different reasons (reviewed by Zeman and Cimprich, 2014). Replication stress triggers the replication stress response, which stabilizes stalled replication forks, halts cell-cycle progression and prevents further firing of replication origins (reviewed by Zeman and Cimprich, 2014). As cells undergoing extrusion are arrested in S-phase, we asked if triggering the replication stress response was important for extrusion. Core components of the replication stress response pathway in *C. elegans* and other metazoans include ATR, Chk1, Rad17, Rad9, Rad1, Hus1, Replication Protein A, TopBP1, Timeless, Tipin and Claspin proteins (Stevens *et al*., 2016; Yazinski and Zou, 2016). RNAi against 7 of the 11 *C. elegans* genes encoding these core components of the replication-stress checkpoint (*atl-1*, *chk-1*, *hpr-9*, *mus-101*, *tim-1*, *tipn-1* and *clsp-1*) produced a Tex phenotype in *ced-3(lf)* animals (Figure 1C, Figure 4L), indicating an involvement of replication stress response in cell extrusion. These findings suggest that the replication stresses underlying the S-phase arrest in extruding cells trigger the replication stress response, which promotes cell extrusion.

Bypassing S-phase arrest and completing the cell cycle prevents cell extrusion

After determining that S-phase arrest is a key feature of cell extrusion, we asked whether the previously identified *C. elegans* cell extrusion regulators *pig-1* (homolog of the mammalian kinase gene *MELK*) and *grp-1* (homolog of the mammalian ARF GEF gene *CYTH3*) (Denning *et al*., 2012) also play a role in

producing this S-phase arrest. We monitored the fate of ABplpappap in *pig-1(RNAi)* embryos by time-lapse confocal microscopy. Strikingly, we found that instead of undergoing S-phase arrest, ABplpappap completed the cell cycle and divided before ventral enclosure in these embryos (Figure 5A; Movie 5). By examining virtual lateral sections, we found that instead of undergoing extrusion, as in the case of control embryos (Figure 5B), ABplpappap in *pig-1(RNAi)* embryos divided to generate daughters that were not extruded (5 of 6 embryos) (Figure 5C). The same fate of ABplpappap was observed in *grp-1(RNAi)* embryos (5 of 5 embryos) (Figure 5D). These findings indicate that in addition to the genes *cye-1* and *cdk-2*, the genes *pig-1* and *grp-1* are required to produce the S-phase arrest that precedes cell extrusion.

Next, we investigated why ABplpappap completed the cell cycle in *pig-1(RNAi)* and *grp-1(RNAi)* embryos. In several cell lineages, such as the Q neuroblast cell lineage, the genes *pig-1* and *grp-1* are required for unequal cell divisions that generate apoptotic cells (Cordes *et al*., 2006; Teuliere *et al*., 2014). Consistent with their function in controlling unequal cell division, RNAi against each of the genes *pig-1* and *grp-1* perturbed the ratio of ABplpappap's size to that of its sister and generated an abnormally large ABplpappap (Figures 5E,F; Supplemental Figures 6A,D,E). These findings indicated that unequal cell division plays an important role in producing the S-phase arrest that precedes cell extrusion. However, despite the requirement for *cye-1* and *cdk-2* to produce this S-phase arrest (Figures 3B, 4B), RNAi against *cye-1* or *cdk-2* did not affect unequal cell division. Neither the size of ABplpappap relative to that of its sister

nor the absolute size of ABplpappap showed a difference among *cye-1(RNAi)*, *cdk-2(RNAi)* and control embryos (Figures 5G,H; Supplemental Figure 6A,B,C). Together, our data indicate that genes required for cell extrusion function to produce the S-phase arrest preceding extrusion either by promoting S-phase entry (via *cye-1* and *cdk-2*) or by preventing cell-cycle completion (via *pig-1* and *grp-1*).

Another difference consistent with the distinct ways by which the cell-cycle genes and unequal-cell-division genes promote cell extrusion was observed in the Tex phenotype caused by RNAi against these genes. Some *pig-1(RNAi)* and *grp-1(RNAi)* animals with the Tex phenotype displayed two supernumerary excretory cells (Figure 5I), presumably because both daughters of ABplpappap adopted the excretory-cell in these animals. By contrast, *cye-1(RNAi)* and *cdk-2(RNAi)* animals with the Tex phenotype displayed only one supernumerary excretory cell (Figure 5I), presumably because ABplpappap did not enter and then complete the cell cycle but rather differentiated directly into an excretory cell.

In short, these findings indicate that the unifying feature of all genes required for cell extrusion is that they function to produce the S-phase arrest observed in cells to be extruded, supporting the conclusion that S-phase arrest is a key requirement of cell extrusion. Either preventing cell-cycle entry or bypassing the S-phase arrest to complete cell division prevented cell extrusion in developing *C. elegans* embryos.

S-phase arrest drives cell extrusion from mammalian epithelial cultures

Since S-phase arrest is the central feature of cell extrusion by *C. elegans* embryo, we asked if S-phase arrest also induces mammalian cell extrusion. We used a monolayer of Madin-Darby Canine Kidney (MDCK) cells as a model of mammalian epithelia and hydroxyurea (HU) as a chemical agent for inducing S-phase arrest. MDCK cells are a simple epithelial system for studies of mammalian cell extrusion in culture (reviewed by Ohsawa *et al*., 2018). HU causes S-phase arrest by inhibiting the enzyme ribonucleotide reductase and depleting deoxyribonucleotides during DNA replication, resulting in stalled DNA replication forks (Timson, 1975; Bianchi *et al*., 1983). We treated MDCK monolayers with either 2 mM HU or vehicle (negative control) for up to 24 h and obtained time-lapse micrographs of the monolayers from this period to assess cell extrusion. Strikingly, cells extruded apically from the MDCK monolayer into the culture medium were three to four times higher in number after HU treatment when compared to the number of cells extruded apically after vehicle treatment (Figure 6A, 6B; Movie 6,7). Next we used MDCK-Fucci cells to determine the cell cycle phase distribution of HU- and vehicle-treated extruded cells (Streichan *et al*., 2014). MDCK-Fucci cells produce a fluorescent signal that varies with the phase of the cell cycle (G0/G1-Red, S/G2/M-Green; Sakaue-Sawano et al., 2008). As expected, most of the HU-treated extruded cells displayed a green fluorescent signal (Figure 6C), indicating that they were in a cell cycle phase subsequent to the onset of DNA replication. We noted that stochastically extruded cells (from vehicle treatment) mostly exhibited red fluorescence

indicative of the G0 or G1 phase (Figure 6D), consistent with the phase of cells that are naturally extruded from post-mitotic zones, such as the tips of intestinal villi (Carroll *et al*., 2018; Eisenhoffer *et al*., 2012).

Since HU is known to increase the rate of apoptosis (Timson, 1975), and agents that promote apoptosis increase the rate of cell extrusion (Andrade and Rosenblatt, 2011), we examined the role of apoptosis in HU-induced cell extrusion. Surprisingly, the fraction of extruded MDCK cells that were apoptotic was not increased by HU treatment (Figure 6D), indicating that HU-induced cell extrusion is not a consequence of an increase in the rate of apoptosis. In addition, we reseeded the extruded MDCK cells in fresh media to measure their viability following HU treatment. We found that the number of viable adherent cells at 2 hours post reseeding was proportional to the number of extrusions for both the HU- and vehicle-treated groups (Figure 6E). Additionally, the number of HU-treated cells doubled at 24 hours post reseeding when compared to 2 hours post reseeding (Figure 6E). Thus, cells extruded by HU treatment were not only viable but also able to resume and complete the cell cycle.

Taken together, the above findings indicate that S-phase arrest drives the extrusion of cells from mammalian epithelia and establish that cell extrusion caused by S-phase arrest is an evolutionarily conserved phenomenon.

DISCUSSION

Here we report that cell cycle S-phase arrest is a cell-intrinsic trigger of cell extrusion and can induce the extrusion of cells of organisms from two divergent branches of the phylogenetic tree - nematodes and mammals. Using

RNAi screens and transgenic cell-cycle reporters, we determined in developing *C. elegans* embryos that perturbations that prevented S-phase arrest blocked cell extrusion. As summarized in Figure 7A, cells destined for extrusion from *ced-3(lf)* embryos are always the smaller daughters of unequal cell divisions. These smaller daughter cells enter S phase of the cell cycle and undergo S-phase arrest, likely because of a deficiency in the energetic and metabolic resources required for DNA synthesis (e.g., nucleotides, replication proteins, etc.). Thus, either bypassing S-phase arrest (by perturbing the process of unequal cell division) and hence completing cell division or preventing S-phase arrest (by blocking cell-cycle entry) prevents cell extrusion in *C. elegans* embryos.

To test the generality of our findings, we used mammalian epithelia treated with HU and showed that S-phase arrest is sufficient to promote cell extrusion. Thus, cell extrusion triggered by S-phase arrest is an evolutionarily conserved mechanism of cell elimination. These observations also demonstrate that cells can be extruded from mitotically active mammalian epithelial tissues. Previous studies of mammalian cell extrusion focused on extrusion from post-mitotic tissues (Rosenblatt *et al*., 2001; Eisenhoffer *et al*., 2012; Gudipaty *et al*., 2017; Saw *et al*., 2017; Kocgozlu *et al*., 2016) or oncogene-driven extrusion from growth-suppressing epithelial environments (Anton *et al*., 2018; Hogan *et al*., 2009; Kajita *et al*., 2010; Leung and Brugge, 2012; Slattum *et al*., 2014; Wu *et al*., 2014).

Our mechanistic model for the evolutionarily conserved process by which S-phase arrest promotes cell extrusion is presented in Figure 7B. In this model, a

mitotically active cell destined for extrusion (i) enters the cell cycle, (ii) arrests in S phase, (iii) loses cell adhesion (see below), and (iv) is extruded as a result of reduced adhesion and forces generated by external morphological or physiological processes.

Why are S-phase arrested cells susceptible to extrusion?

We observed previously that cells extruded by *C. elegans* embryos do not express the classical E-cadherin HMR-1 and other cell-adhesion molecules (Denning *et al*., 2012). The absence of such adhesion molecules likely allows cells to be squeezed out of the embryo by morphological forces generated by migrating hypodermal cells and neighboring neuroblasts during ventral enclosure (Chisholm and Hardin, 2005; Wernike *et al*., 2016). Consistent with this view, the loss of E-cadherin-mediated adhesion caused by cleavage of the extracellular part of a cell's E-cadherin molecules is sufficient to drive cell extrusion from an MDCK monolayer (Grieve and Rabouille, 2014). We speculate that a signaling pathway initiated by S-phase arrest downregulates the expression of cell adhesion molecules in cells destined for extrusion. Indeed, in HeLa cell cultures, cell adhesion increases during S phase via the activity of the cell-cycle regulator CDK1 and decreases later in the cell cycle upon inhibition of CDK1 by Wee1 (Jones *et al*., 2018). Interestingly, activation of the replication stress response, which is required for cell extrusion in *C. elegans* (Figure 1C, 4L), blocks CDK1 activity (Jin *et al*., 2003; Mailand *et al*., 2002; Xiao *et al*., 2003). Furthermore, HU-mediated S-phase arrest also inactivates CDK1 in MDCK cells (Anton *et al*., 2018). We therefore propose that a reduction in CDK1 activity following S-phase

arrest decreases cell adhesion, thereby facilitating the extrusion of cells subjected to external forces from cellular neighbors.

Extrusion of S-phase arrested cells is likely tumor-suppressive

Replication forks under prolonged S-phase arrest can collapse and produce DNA damage, genomic rearrangements and ploidy defects, all of which are associated with oncogenesis (reviewed by Gaillard *et al*., 2015). The human genes that promote replication stress and S-phase arrest are frequently amplified, overexpressed or activated by mutations in tumors (Otto and Sicinski, 2017). Cells in such tumors experience persistent replication stress that can lead to S-phase arrest (Gaillard *et al*., 2015). Hence, tumor cells and cells with oncogenic potential might well be eliminated via cell extrusion, in which case the extrusion of cells arrested in S phase would be tumor-suppressive. We propose that cell extrusion driven by S-phase arrest is a checkpoint mechanism that functions to eliminate cells at all stages of the oncogenic transformation process, ranging from precancerous cells in S-phase arrest to tumor cells in a malignant tumor.

Subversion of cell extrusion driven by S-phase arrest might contribute to metastasis

Inactivation of either $S1P_2$ or the tumor suppressor APC or expression of oncogenic K-Ras changes the direction of cell extrusion from apical, which favors cell elimination by extrusion into the lumen, to basal, which favors dissemination of extruded cells to surrounding tissue (Gu *et al*., 2015; Marshall *et al*., 2011; Slattum *et al*., 2014). Mutations in these genes are hallmarks of metastatic

433 tumors. While cell extrusion caused by S-phase arrest likely can suppress tumor
434 development, the same mechanism of cell extrusion might paradoxically promote
435 cancer metastasis if the extrusion direction changes from apical to basal. We
436 observed that cells subjected to HU-mediated extrusion failed to die (Figure 6D)
437 and instead were capable of reentering the cell cycle and proliferating (Figure
438 6E). Thus, basal extrusion of cells arrested in S-phase might facilitate metastasis
439 by disseminating live tumor cells arrested in S phase to other tissues and organs.
440 We propose that mutations in genes, such as $S1P_2$, APC and K-Ras, promote
441 metastasis by facilitating the basal extrusion and spread of tumor cells arrested
442 in S phase.

443 In summary, we have discovered a novel conserved mechanism that links
444 a cell-cycle vulnerability to the process of cell extrusion. We suggest that cell
445 extrusion mediated by S-phase arrest is a mechanism of cell elimination common
446 to all metazoa. These findings have implications for the field of cancer biology, as
447 cell extrusion caused by S-phase arrest likely regulates both the survival and
448 spread of tumor cells.
449

ACKNOWLEDGMENTS

We thank S. van den Heuvel for providing strains; the CGC, which is funded by NIH Office of Research Infrastructure Programs (P40 OD010440), for providing some strains; N. An and T. Ljungars for strain management; S. Luo, S.R. Sando, A. Doi, and A. Corrionero and other members of the Horvitz laboratory for helpful discussions, and D. Ghosh, C.L. Pender, J.N. Kong, M.G. Vander Heiden, P.W. Reddien, R.O. Hynes for suggestions regarding the manuscript. V.K.D. was a Howard Hughes Medical Institute International Student Research fellow. C.P.P. is the recipient of a Human Frontiers Science Program postdoctoral fellowship (LT000654/2019-L). J.R. and C.P.P. were funded by King's College London startup funds. H.R.H. is the David H. Koch Professor of Biology at MIT and an Investigator at the Howard Hughes Medical Institute.

AUTHOR CONTRIBUTIONS

H.R.H. supervised the project. V.K.D. and H.R.H. conceptualized the project. V.K.D. and H.R.H. designed the experiments that used *C. elegans*. V.K.D. and R.D. performed the experiments that used *C. elegans*. V.K.D., R.D. and D.P.D. generated reagents. C.P. and J.R. designed the experiments that used mammalian cells. C.P. performed the experiments that used mammalian cells. V.K.D., D.P.D. and H.R.H. wrote the original manuscript draft. All authors contributed to data analysis, interpretation, and reviewing and editing of the manuscript.

Declaration of Interests

The authors declare no competing interests.

Figure 1

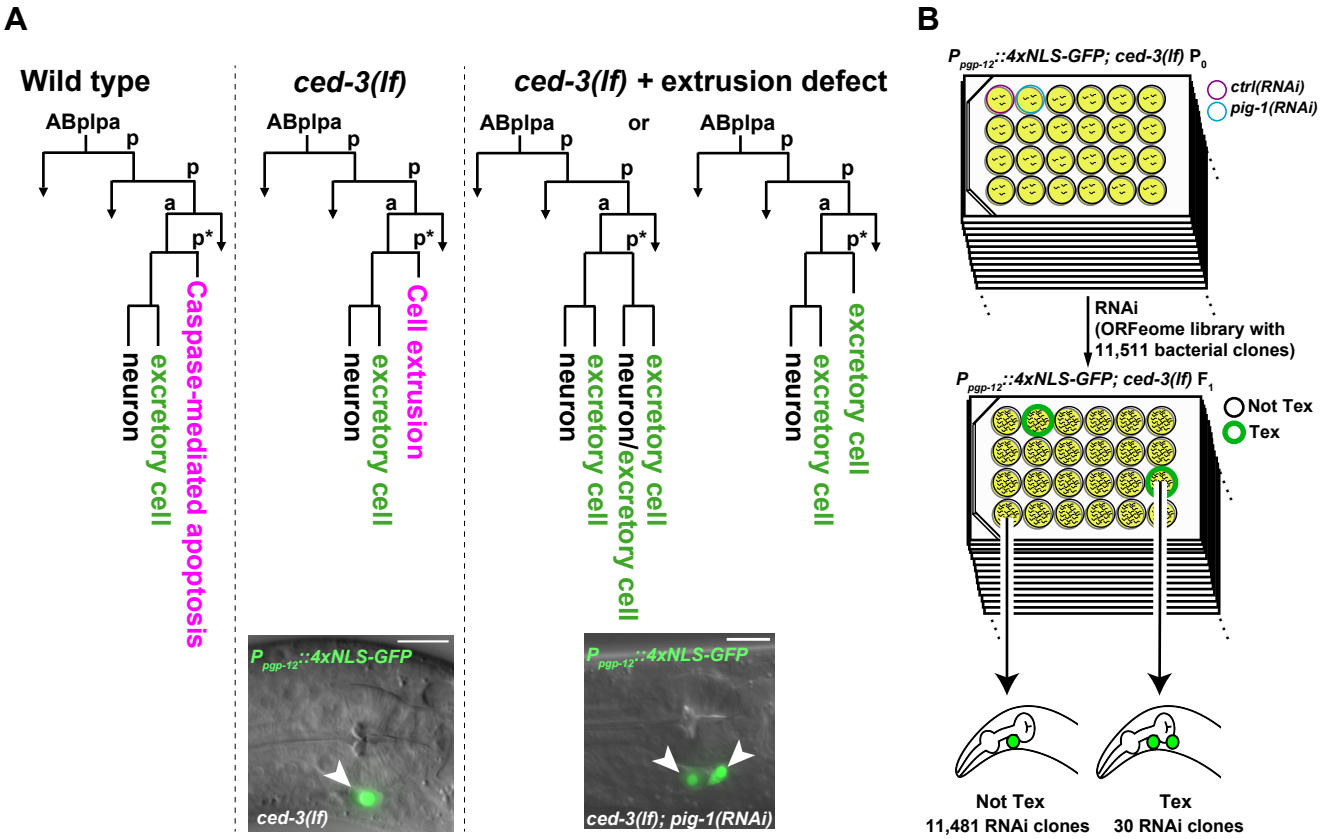

C

Cell cycle genes with a candidate role in cell extrusion based on RNAi-induced Tex phenotype

RNAi target gene	% Tex (n)	Mammalian homolog	G1/S Role	Role/Function in cell cycle
Control	1 (107)	-	-	-
cdc-25.2‡	21(159)	CDC25	Yes	Protein phosphatase that removes inhibitory phosphorylations from cyclin dependent kinases (CDKs) 1 and 2
cya-1‡	12 (363)	Cyclin A	Yes	Protein that binds to CDK2 to regulate S-phase progression and to CDK1 to regulate progression through G2 and M phases
cye-1‡	87 (165)	Cyclin E	Yes	Protein that binds to CDK2 to regulate transition from G1 to S phase of the cell cycle
cdk-1‡	15 (61)	CDK1	Yes	CDK that can bind to multiple cyclin proteins to phosphorylate targets for the positive regulation of cell cycle progression
cdk-2	65 (181)	CDK2	Yes	CDK that binds to Cyclins E and A to promote S-phase entry and progression, respectively
psf-1‡ *psf-2*‡ *psf-3*‡	36 (116) 39 (156) 50 (105)	GINS Complex	Yes	Proteins that function as components of a complex that is involved in DNA replication origin firing and replication progression
csn-1‡ *csn-4*‡ *csn-5*‡	43 (132) 47 (141) 39 (145)	COP9 Signalosome	Maybe	Proteins that function as components of a complex that is required for the function of SCF E3 ligases that regulate the cell cycle
atl-1 *chk-1*	9 (444) 9 (220)	ATR Chk1	Yes	Proteins that function in the replication stress checkpoint response

‡Genes identified from the genome-scale RNAi screen

Figure 1 A Genome-wide RNAi screen for genes required for cell extrusion identifies multiple cell-cycle genes

(A) Lineage diagrams show the fate of the cell ABplpappap (marked with an *) in embryos that are wild-type, embryos with a *ced-3(lf)* mutation and embryos with a *ced-3(lf)* mutation and a defect in cell extrusion. A micrograph of the pharyngeal region showing excretory cell(s), which express nuclear GFP and are marked with white arrowhead(s), is shown for a representative *ced-3(lf)* animal and a *ced-3(lf)* + extrusion defect (*ced-3(lf); pig-1(RNAi)*) animal below the corresponding cell-lineage diagrams. Scale bar, 10 μm.

(B) Schematic representation of the genome-wide RNAi screen for the Tex phenotype.

(C) RNAi clone targets with a function in the cell cycle identified from the genome-wide or candidate-based RNAi screens for the Tex phenotype and the corresponding penetrance of the Tex phenotype. The mammalian homologs of these genes and their functions in mammals are shown. G1/S Role indicates whether an identified RNAi target has a role in G1, G1-to-S phase transition or S-phase progression in mammals. ‡, genes identified from the genome-wide RNAi screen; other genes were identified from a candidate RNAi screen of cell cycle genes for the Tex phenotype (Supplemental Table 1).

Figure 2

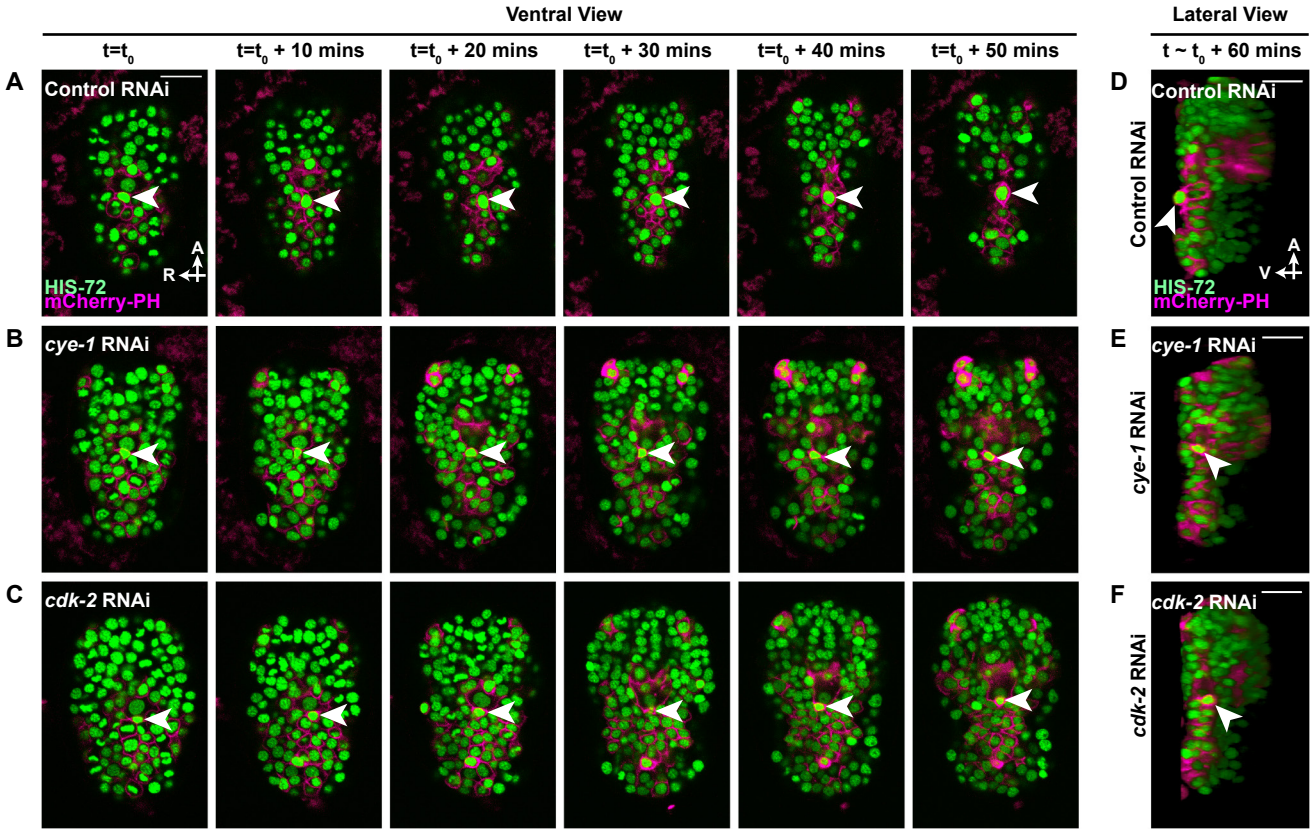

493 **Figure 2 Cell extrusion of ABplpappap requires the function of the cell-**

494 **cycle genes *cye-1* and *cdk-2***

495 (A-C) Micrographs of the ventral surface obtained at 10-min intervals over a

496 period of 50 min using time-lapse confocal microscopy show the location of

497 ABplpappap (arrowhead) on the ventral surface with respect to other embryonic

498 cells in (A) control, (B) *cye-1(RNAi)*, and (C) *cdk-2(RNAi)* embryos. The embryos

499 shown carried the transgenes *stIs10026* and *nIs632*. A, anterior; R, right. Scale

500 bar, 10 μm.

501 (D-F) Virtual lateral sections through the ABplpappap cell in *ced-3(lf)* embryos

502 show the relative location of ABplpappap (arrowhead) in (D) control, (E) *cye-*

503 *1(RNAi)*, and (F) *cdk-2(RNAi)* embryos. Embryos shown in (D), (E) and (F) are

504 the same as those in (A), (B) and (C), respectively. A, anterior; V, ventral. Scale

505 bar, 10 μm.

506

Figure 3

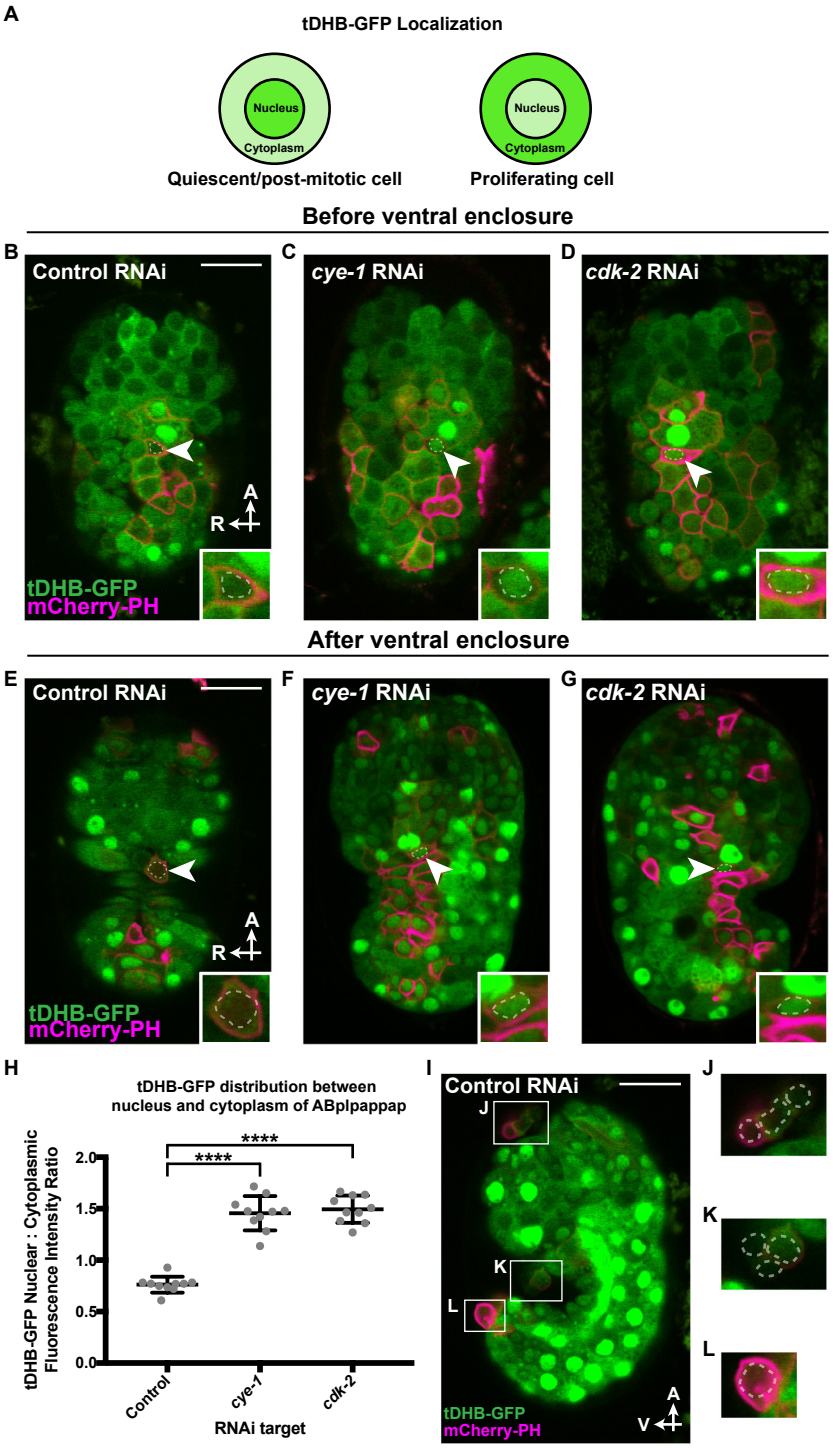

Figure 3 Cells that are extruded enter the cell cycle and are extruded in a *cye-1*- and *cdk-2* -dependent manner

(A) Schematic showing the relative nuclear/cytoplasmic localization of a truncated DHB (tDHB) – GFP fusion protein in a quiescent/post-mitotic cells and in cells between S phase and mitosis in the cell cycle (van Rijnberk *et al*., 2017).

(B-G) Micrographs of the ventral surface, including ABplpappap (arrowhead), of *ced-3(lf)* embryos expressing tDHB-GFP obtained (B-D) prior to and (E-G) post ventral enclosure using confocal microscopy in (B,E) control embryos, (C,F) *cye-1 (RNAi)* embryos, and (D,G) *cdk-2(RNAi)* embryos. Inset, a magnified view of the ABplpappap cell. The ABplpappap nucleus, as determined by Nomarski optics, is marked by a dotted line in each image and inset. The embryos shown carried transgenes *heSi192* and *nIs861*. A, anterior; R, right. Scale bar, 10 μm.

(H) Quantification of the ratio of tDHB-GFP fluorescence intensity in the nucleus to that in the cytoplasm in control, *cye-1(RNAi)*, or *cdk-2(RNAi)* embryos expressing tDHB-GFP. ****, $p<0.0001$ per ordinary one-way ANOVA of the log of ratios. n=10 embryos per RNAi treatment.

(I-L) Micrograph of (I) a *ced-3(lf)* embryo expressing tDHB-GFP obtained at the comma stage using confocal microscopy. Magnified views are provided for the cells extruded at (J) the anterior sensory depression, (K) the ventral pocket, and (L) the posterior tip of the embryo, with the corresponding regions outlined in (I). The cell nucleus, as determined by Nomarski optics, is marked by a dotted line for each extruded cell in the magnified images (J), (K) and (L). The embryo

529 shown carried the transgenes *heSi192* and *nIs861*. A, anterior; V, ventral. Scale

530 bar, 10 µm.

531

Figure 4

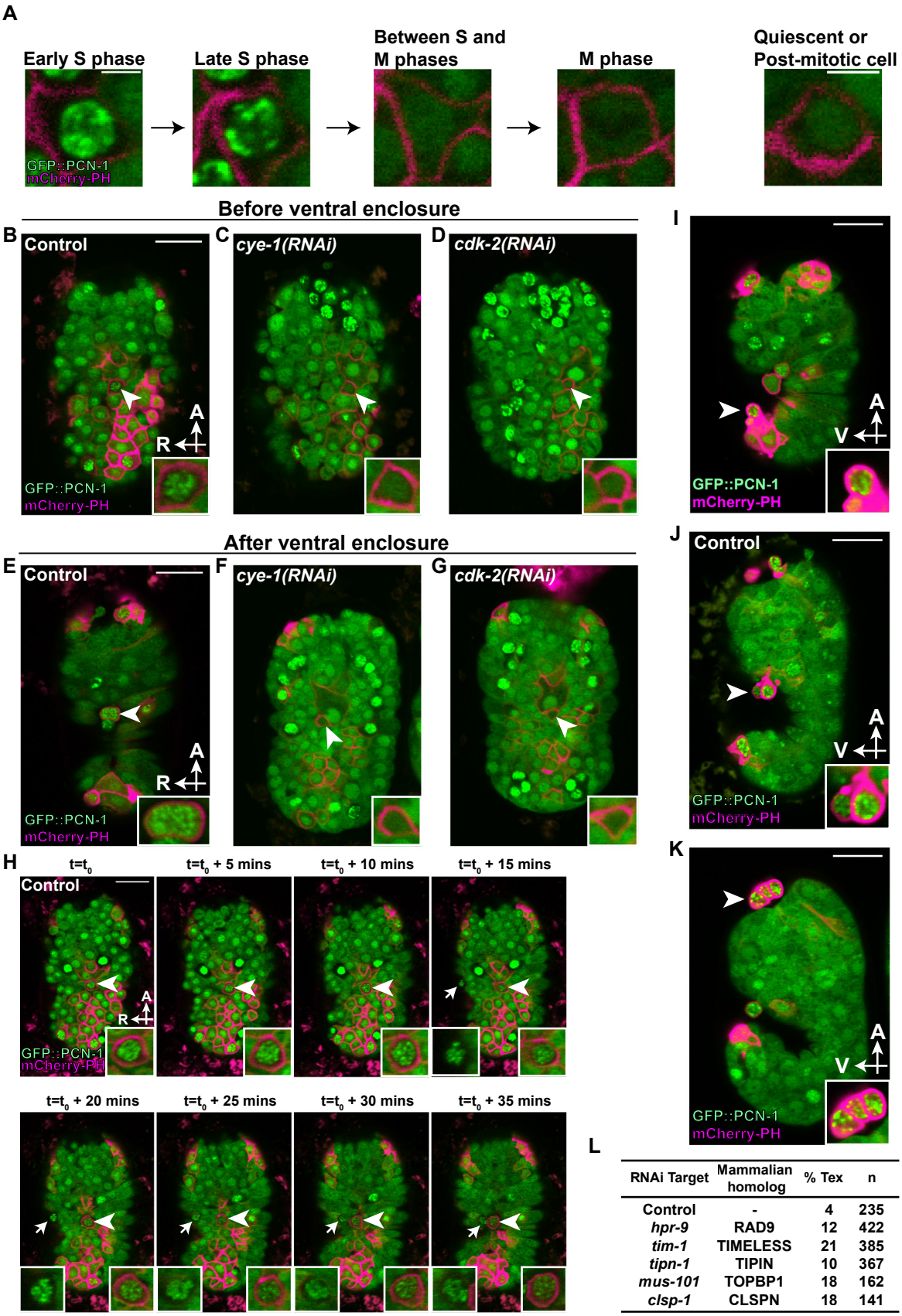

RNAi Target	Mammalian homolog	% Tex	n
Control	-	4	235
hpr-9	RAD9	12	422
tim-1	TIMELESS	21	385
tipn-1	TIPIN	10	367
mus-101	TOPBP1	18	162
clsp-1	CLSPN	18	141

Figure 4 Cells undergoing extrusion arrest in S phase and trigger the DNA replication stress checkpoint

(A) Representative micrographs showing localization patterns of GFP::PCN-1 in the same cell at different phases of the cell cycle or in a different cell in a post-mitotic state. The post-mitotic cell shown is ABplpappaaa (future RMEV neuron). These cells were imaged from a *ced-3(lf)* embryo, which carried the transgenes *nIs861* and *isIs17*. Scale bar, 2 μm.

(B-G) Micrographs of the ventral surface, including ABplpappap (arrowhead), of *ced-3(lf)* embryos expressing GFP::PCN-1 obtained (B-D) prior to and (E-G) post ventral enclosure using confocal microscopy in (B,E) control embryos, (C,F) *cye-1(RNAi)* embryos, and (D,G) *cdk-2(RNAi)* embryos. Inset, a magnified view of ABplpappap. The embryos shown carried the transgenes *nIs861* and *isIs17.* A, anterior; R, right. Scale bar, 10 μm.

(H) Micrographs obtained at 5-min intervals using time-lapse confocal microscopy show the GFP::PCN-1 localization pattern in ABplpappap (arrowhead) and another unidentified extruded cell (arrow) as they were progressively extruded over 35 min in a *ced-3(lf)* embryo with control RNAi. Left insets, magnified views of unidentified extruded cell; right insets, magnified views of ABplpappap. The embryo shown carried the transgenes *isIs17* and *nIs861*. The decrease in fluorescence intensity can be attributed to bleaching from repeated imaging over time. A, anterior; R, right. Scale bar, 10 μm.

(I-K) Micrographs of extruded cells in *ced-3(lf)* embryos expressing GFP::PCN-1 obtained at the comma stage using confocal microscopy show GFP::PCN-1

555 localization in cells at (I) the posterior tip of the embryo (no RNAi), (J) the ventral
556 pocket (control RNAi), and (K) the anterior sensory depression (no RNAi). Inset,
557 a magnified view of extruded cells marked by an arrowhead. The embryos shown
558 carried the transgenes *isIs17* and *nIs861*. A, anterior; V, ventral. Scale bar, 10
559 μm.
560 (L) Penetrances of the Tex phenotype produced by RNAi-mediated targeting of
561 replication-stress checkpoint genes *hpr-9*, *tim-1*, *tipn-1*, *mus-101* and *clsp-1* in
562 *ced-3(lf)* animals. The strain used for scoring the RNAi-induced Tex phenotype
563 carried the transgene *nIs433*, which expresses nuclear GFP in excretory cell(s).
564

Figure 5

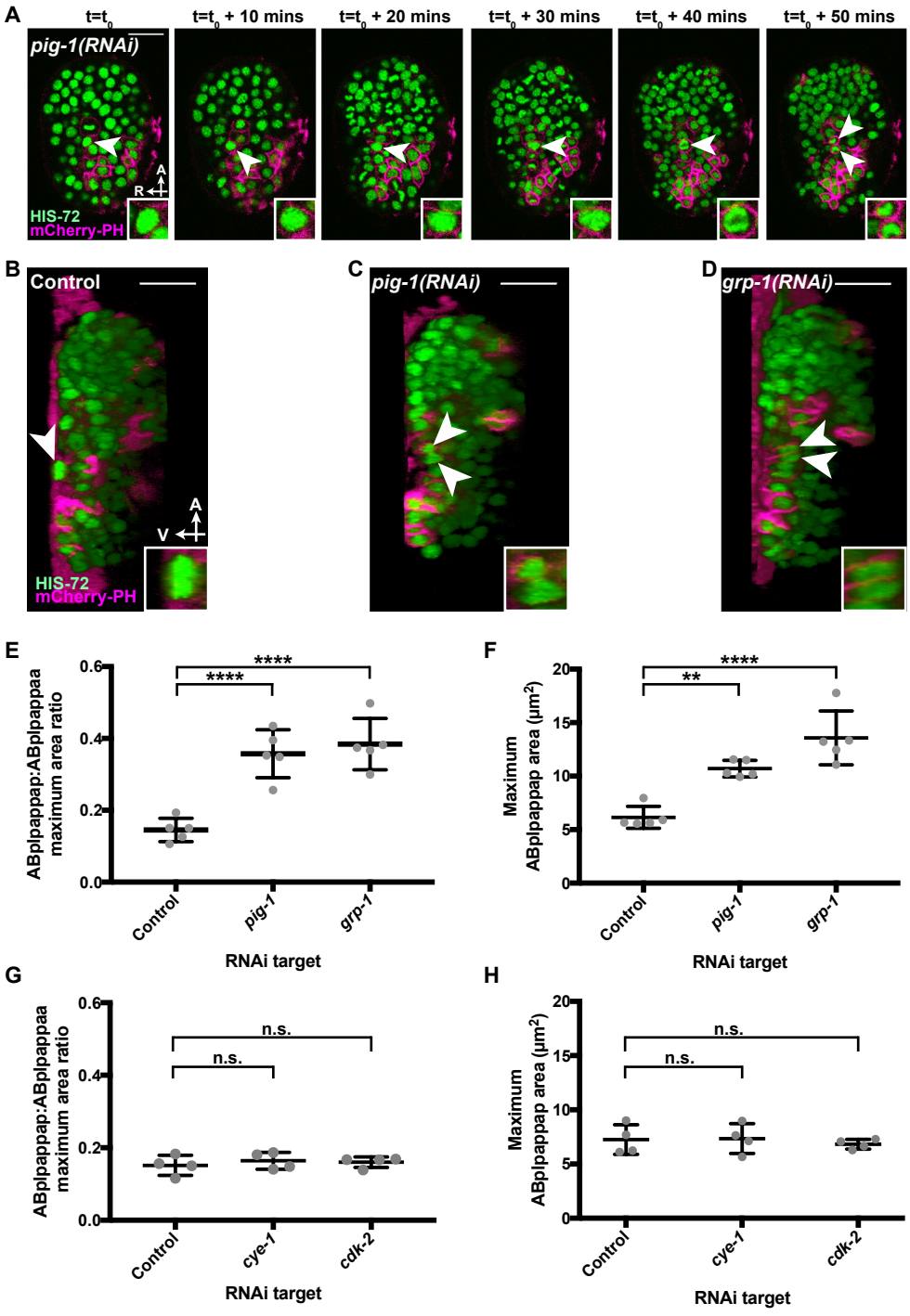

I

RNAi Target	% Tex	No. of animals			Total no. of animals
Control	1	171	1	0	172
pig-1	74	50	106	39	195
grp-1	83	32	103	54	189
cye-1	75	58	170	0	228
cdk-2	77	54	177	0	231

Figure 5 Unequal cell division genes *pig-1* and *grp-1* promote extrusion by preventing cell-cycle progression beyond S phase

(A) Micrographs of a *pig-1(RNAi)* embryo obtained at 10-min intervals over a period of 50 min using time-lapse confocal microscopy show that an enlarged ABplpappap divides before ventral enclosure in *pig-1(RNAi)* embryos. The embryo shown carried the transgenes *stIs10026* and *nIs861*. Inset, a magnified view of ABplpappap or its descendants. A, anterior; R, right. Scale bar, 10 μm.

(B-D) Virtual lateral sections of *ced-3(lf)* embryos through ABplpappap (single arrowhead) or its daughters (two arrowheads) in a (B) control embryo, (C) *pig-1(RNAi)* embryo, and (D) *grp-1(RNAi)* embryo. Inset, a magnified view of ABplpappap or its descendants. The embryos shown carry the transgenes *stIs10026* and *nIs861*. A, anterior; V, ventral. Scale bar, 10 μm.

(E) Ratio of maximum area (see Materials and methods) of ABplpappap to that of its sister in *ced-3(lf)* embryos with RNAi against control, *pig-1* or *gpr-1*. Error bars, standard deviation. ****, $p<0.0001$ per ordinary one-way ANOVA of log of ratios. n=5 embryos for each RNAi treatment.

(F) Quantification of the maximum area (see Materials and methods) of ABplpappap in control embryos, *pig-1(RNAi)* embryos and *grp-1(RNAi)* embryos. Error bars, standard deviation. **, $p<0.01$; ****, $p<0.0001$ per ordinary one-way ANOVA. n=5 embryos for each RNAi treatment.

(G) Ratio of maximum area (see Materials and methods) of ABplpappap to that of its sister in *ced-3(lf)* embryos with RNAi against control, *cye-1* or *cdk-2*. Error

587 bars, standard deviation. n.s., not significant per ordinary one-way ANOVA of log
588 of ratios. n=4 embryos for each RNAi treatment.
589 (H) Quantification of the maximum area (see Materials and methods) of
590 ABplpappap in control embryos, *cye-1(RNAi)* embryos and *cdk-2(RNAi)*
591 embryos. Error bars, standard deviation. n.s., not significant per ordinary one-
592 way ANOVA. n=4 embryos for each RNAi treatment.
593 (I) Penetrances of the Tex phenotype and number of animals with one, two or
594 three excretory cells produced by RNAi against genes identified from genetic
595 screens for defective extrusion. The *ced-3(lf)* strain used for this experiment
596 carries the transgene *nIs433*.
597

Figure 6

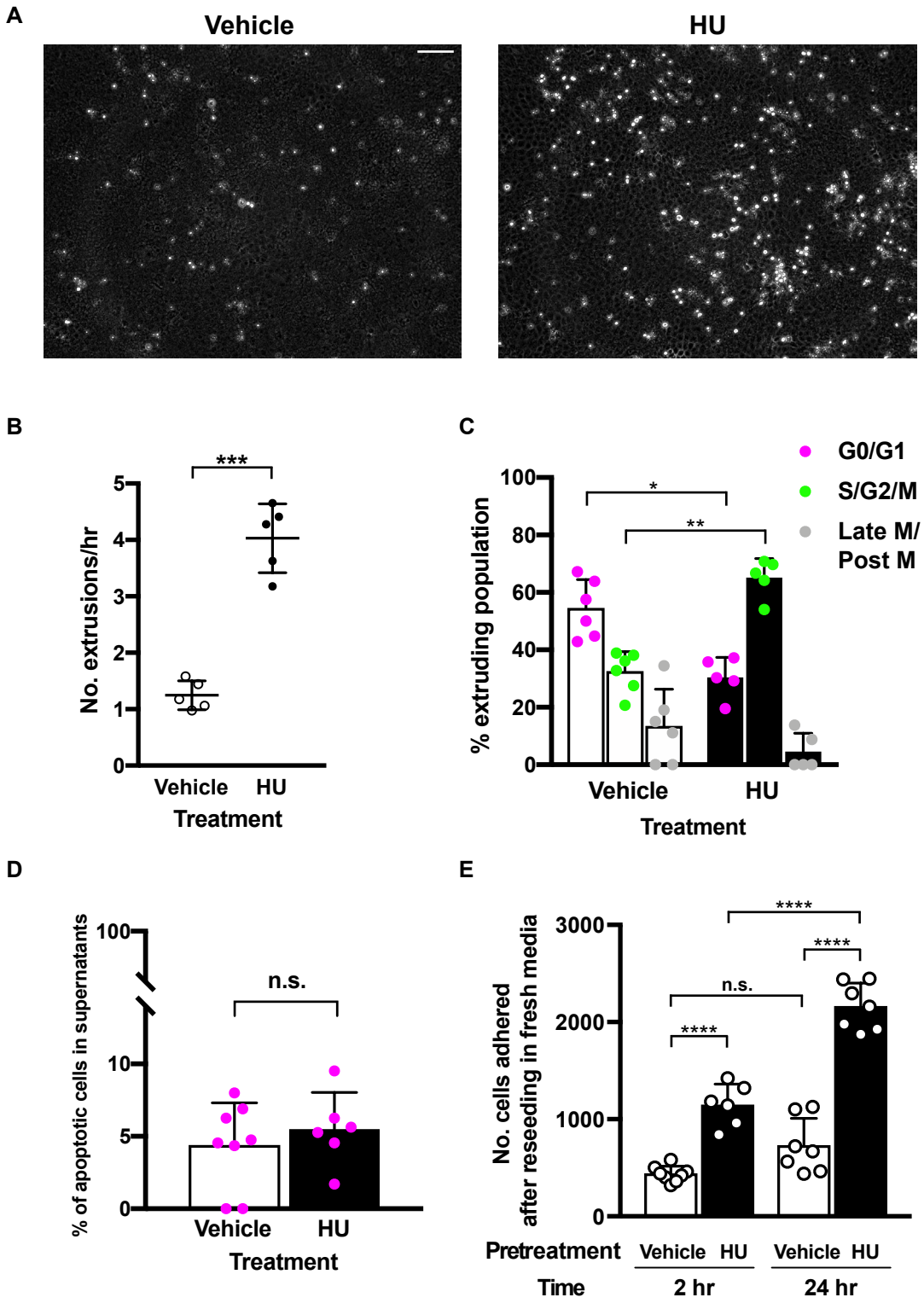

598 **Figure 6 S-phase arrest is sufficient for cell extrusion from a simple**
599 **mammalian epithelial layer**

600 (A) Representative images from time-lapse videos of mammalian MDCK cell
601 monolayers exposed to either vehicle or 2 mM hydroxyurea (HU) at 22 h of
602 exposure. Extruded cells can be identified as bright, white, rounded spots rising
603 from the epithelial plane. Many more extruded cells are observed after HU
604 treatment as compared to vehicle treatment. Scale bar, 100 μm.

605 (B) Graph showing average number of cell extrusions per h in vehicle-treated
606 and 2 mM HU-treated MDCK monolayers. Each data point represents a separate
607 experiment conducted for up to 24 h normalized by duration of experiment for
608 comparison. Error bars, standard deviation. ***, $p < 0.001$ per Welch's two-tailed
609 t-test. n=5 measurements experimental replicates for each condition.

610 (C) Graph showing cell cycle phase distribution of extruded MDCK-FUCCI cells
611 after HU treatment or vehicle treatment. Each data point represents a separate
612 experiment. Error bars, standard deviation. *, $p<0.05$; **, $p<0.01$ per Kruskal-
613 Wallis test.

614 (D) Graph showing percentage of cells extruded after vehicle treatment or HU
615 treatment that are apoptotic as per Trypan blue uptake. Each data point
616 represents a separate experiment. Error bars, standard deviation. n.s., not
617 significant per Mann-Whitney test.

618 (E) Graph showing the number of HU-treated or vehicle-treated extruded cells
619 that adhered at 2 h and 24 h after reseeding in fresh media. Each data point

620 represents a separate experiment. Error bars, standard deviation. n.s., not
621 significant; ****, p<0.0001 per standard one-way ANOVA.
622

Figure 7

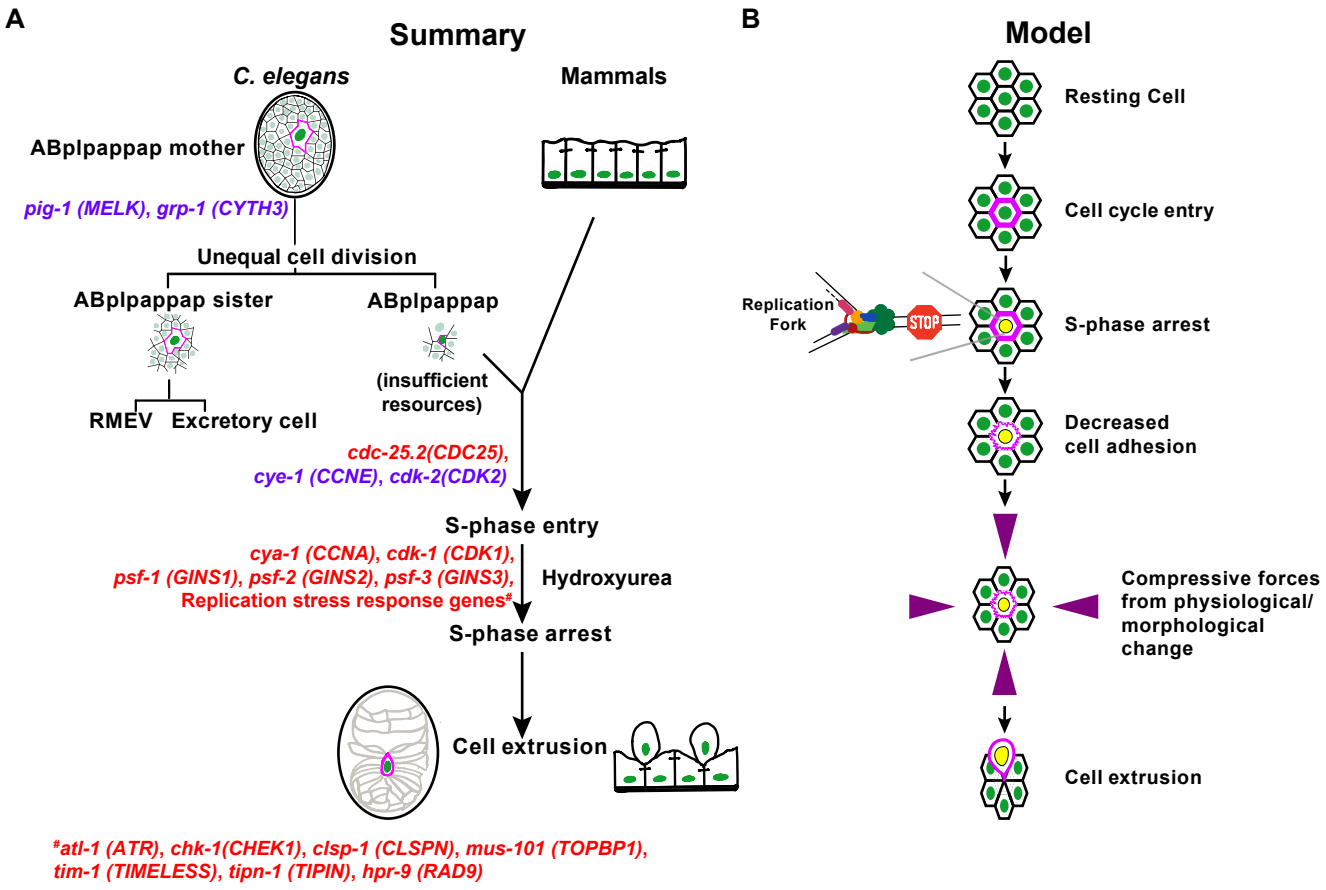

Figure 7 Summary and Model: S-phase arrest drives cell extrusion

(A) A summary of the genes required for cell extrusion by *C. elegans*, their mammalian homologs (in parentheses) and their associated biological processes that precede the S-phase arrest that drives the cell extrusion of ABplpappap (and other extruded cells) from *C. elegans* embryos. Treatment of mammalian cells (MDCK) with HU chemically produces an S-phase arrest in cells that drives their extrusion from simple epithelial layers, as shown. At each step preceding cell extrusion by *C. elegans*, genes with function we demonstrated to occur at the corresponding step are shown in purple, and genes with probable function at that step are shown in red. Relevant cells in the *C. elegans* embryos are outlined in magenta. The horizontal hyphen-like lines connecting mammalian cells indicate adhesion junctions.

(B) Model: A cell that enters the cell cycle (marked by magenta cell boundary) but arrests in S phase (marked by yellow nucleus) will have lowered cell adhesion (marked by wavy magenta cell boundary). When a cell with lowered cell adhesion caused by S-phase arrest experiences morphological or physiological forces (marked by purple arrows) that cause a squeezing-like effect, the cell gets extruded.

Supplemental Table 1

RNAi target	Mammalian Homolog	%Tex	n	extensive lethality?
empty vector	-	1	159	N
atl-1	ATR	10	509	N
cdc-14	CDC14	1	168	N
cdc-25.1	CDC25	0	111	Y
cdc-25.2	CDC25	12	159	N
cdc-25.3	CDC25	2	168	N
cdc-25.4	CDC25	0	183	N
cdk-1	CDK1	15	61	Y
cdk-11.1	CDK11	0	175	N
cdk-11.2	CDK11	1	132	N
cdk-12	CDK12	0	167	N
cdk-2	CDK2	65	181	N
cdk-4	CDK4	1	193	N
cdk-5	CDK5	0	155	N
cdk-7	CDK7	0	130	Y
cdk-8	CDK8	1	186	N
cdk-9	CDK9	1	155	Y
cdt-1	CDT1	1	147	Y
chk-1	CHEK1	10	164	Y
cit-1.1	CCNT1/2	0	105	N
cit-1.2	CCNT1/2	1	244	N
cki-1	CDKN1	0	125	N
cki-2	CDKN1	1	216	N
clk-2	TELO2	1	156	N
cul-1	CUL1	5	81	Y
cul-2	CUL2	0	21	Y
cul-3	CUL3	5	151	Y
cul-4	CUL4	0	141	N
cya-1	CCNA	20	309	N
cyb-1	CCNB1	4	136	N
cyb-2.1	CCNB2	1	102	N
cyb-2.2	CCNB2	0	144	N
cyb-3	CCNB3	14	7	Y

RNAi target	Mammalian Homolog	%Tex	n	extensive lethality?
cic-1	CCNC	1	158	N
cyd-1	CCND	0	111	N
cye-1	CCNE	89	133	Y
cyh-1	CCNH	0	119	Y
cyl-1	CCNL	1	106	Y
cyy-1	CCNY	1	108	N
dpl-1	TFDP1	0	167	N
efl-1	E2F	0	141	N
emb-27	CDC16	0	107	Y
emb-30	ANAPC4	0	130	Y
fzr-1	FZR1	1	146	N
fzy-1	CDC20	0	130	Y
hpr-17	RAD17	5	214	N
hus-1	HUS1	0	132	N
lin-15	-	1	104	N
lin-23	βTrCP	23	147	N
lin-35	Rb	0	134	N
lin-36	-	0	111	N
lin-9	LIN9	1	125	N
mat-1	CDC27	0	80	Y
mat-2	ANAPC1	1	163	Y
mat-3	CDC23	0	108	Y
mdf-1	MAD1L1	3	112	N
mdf-2	MAD2L1	1	111	N
mrt-2	RAD1	0	114	N
rnr-1	RRM1	5	103	Y
san-1	BUB1B	1	145	N
wee-1.1	PKMYT1	1	159	N
wee-1.3	PKMYT1	0	60	Y

642 **Supplemental Table 1 Penetrance of the Tex phenotype produced by RNAi**
643 **against cell cycle genes (and non-cell-cycle cyclins and CDKs) in *ced-3(lf)***
644 **animals.** Tex penetrance produced by each of the RNAi clones in the cell-cycle
645 RNAi library, the number of animals counted for each RNAi clone and whether or
646 not the RNAi clone produced extensive lethality are shown. Genes corresponding
647 to RNAi clones that produced more than 9% penetrance of the Tex phenotype
648 are in bold. *cyb-3* did not fit this criterion, as extensive lethality prevented the
649 counting of sufficient number of animals to assign significance. Some cyclins and
650 CDKs that function outside the cell cycle were included in this library and served
651 as negative controls.
652

Supplemental Table 2

RNAi target	Mammalian Homolog	%Tex	n
empty vector	-	0	127
atl-1	ATR	0	198
cdc-25.2	CDC25	0	36
cdk-1	CDK1	0	51
cdk-2	CDK2	0	237
chk-1	CHK1	0	115
csn-1	GPS1	0	156
csn-4	COPS4	0	141
csn-5	COPS5	0	114
cya-1	CCNA	0	167
cye-1	CCNE	0	143
lin-23	βTrCP	12	96
psf-1	GINS1	0	150
psf-2	GINS2	0	190
psf-3	GINS3	0	72

Supplemental Table 2 Penetrance of the Tex phenotype produced in wild-type animals by RNAi against cell cycle genes with potential roles in cell extrusion. The Tex penetrance produced in wild-type animals by RNAi clones against cell cycle genes that might be involved in cell extrusion (based on the corresponding Tex penetrance in *ced-3(lf)* animals) is provided. *Bona fide* candidates for cell extrusion regulation should not produce a Tex phenotype in wild-type animals, as cell extrusion does not occur in wild-type worms. A Tex phenotype in wild-type animals could occur from other effects of RNAi against cell cycle genes, such as excessive proliferation leading to multiple excretory cells. Such proliferation is likely the case for *lin-23*, as RNAi against *lin-23* has been previously described to cause excessive proliferation (Kipreos *et al*., 2000). The 13 other genes are good candidates to be regulators of cell extrusion by the criterion of dependence of the Tex phenotype on the loss of function of *ced-3*.

Supplemental Figure 1

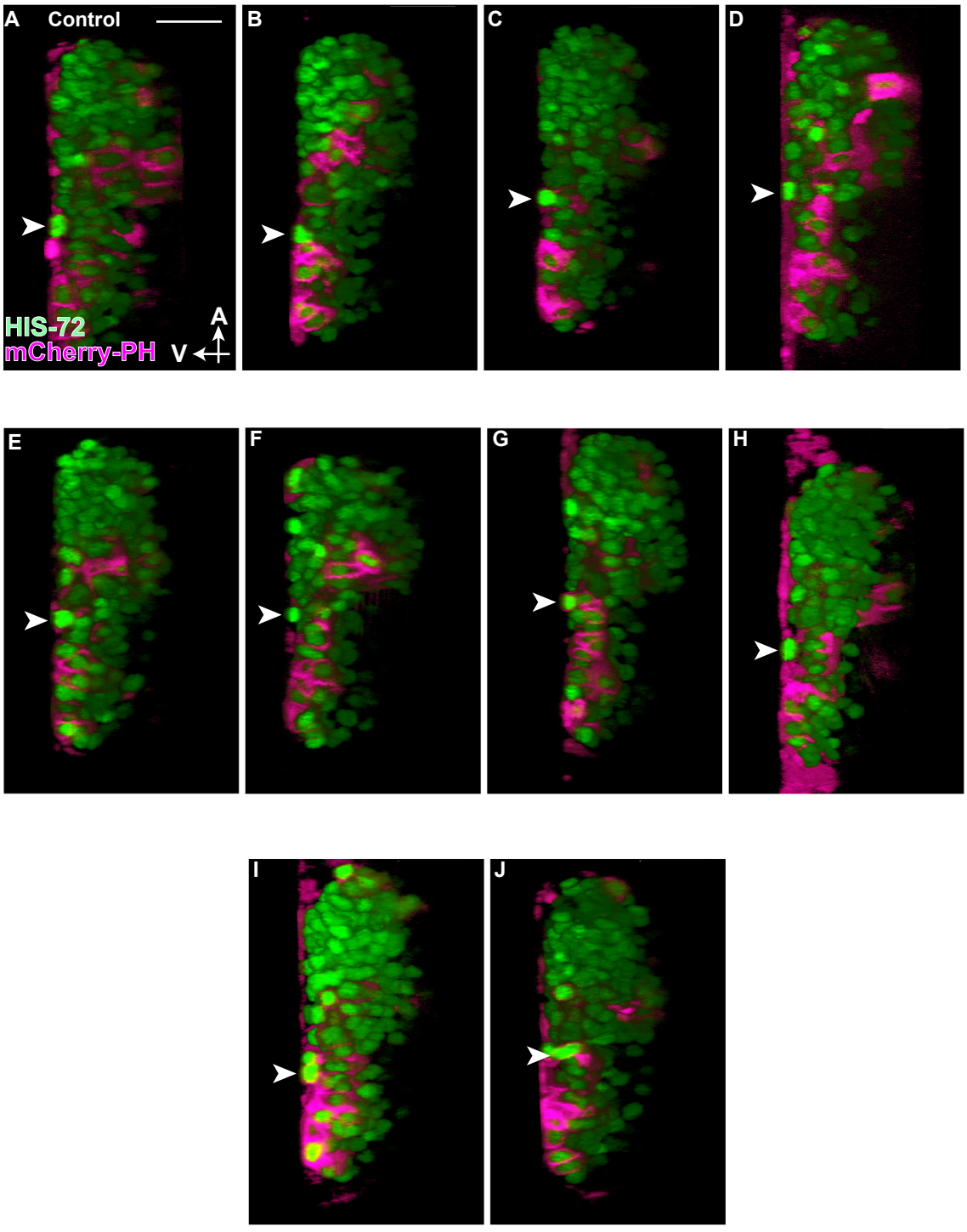

Supplemental Figure 1 ABplpappap is extruded by control embryos

(A-J) Virtual lateral sections of embryos through the ABplpappap cell (arrowhead) in (A-J) 10 control embryos show (A-I) ABplpappap is extruded in 9 of 10 embryos and (J) is not extruded in 1 of 10 embryos. The embryos shown carry the transgenes *stIs10026* and *nIs861*. A, anterior; V, ventral. Scale bar, 10 μm.

Supplemental Figure 2

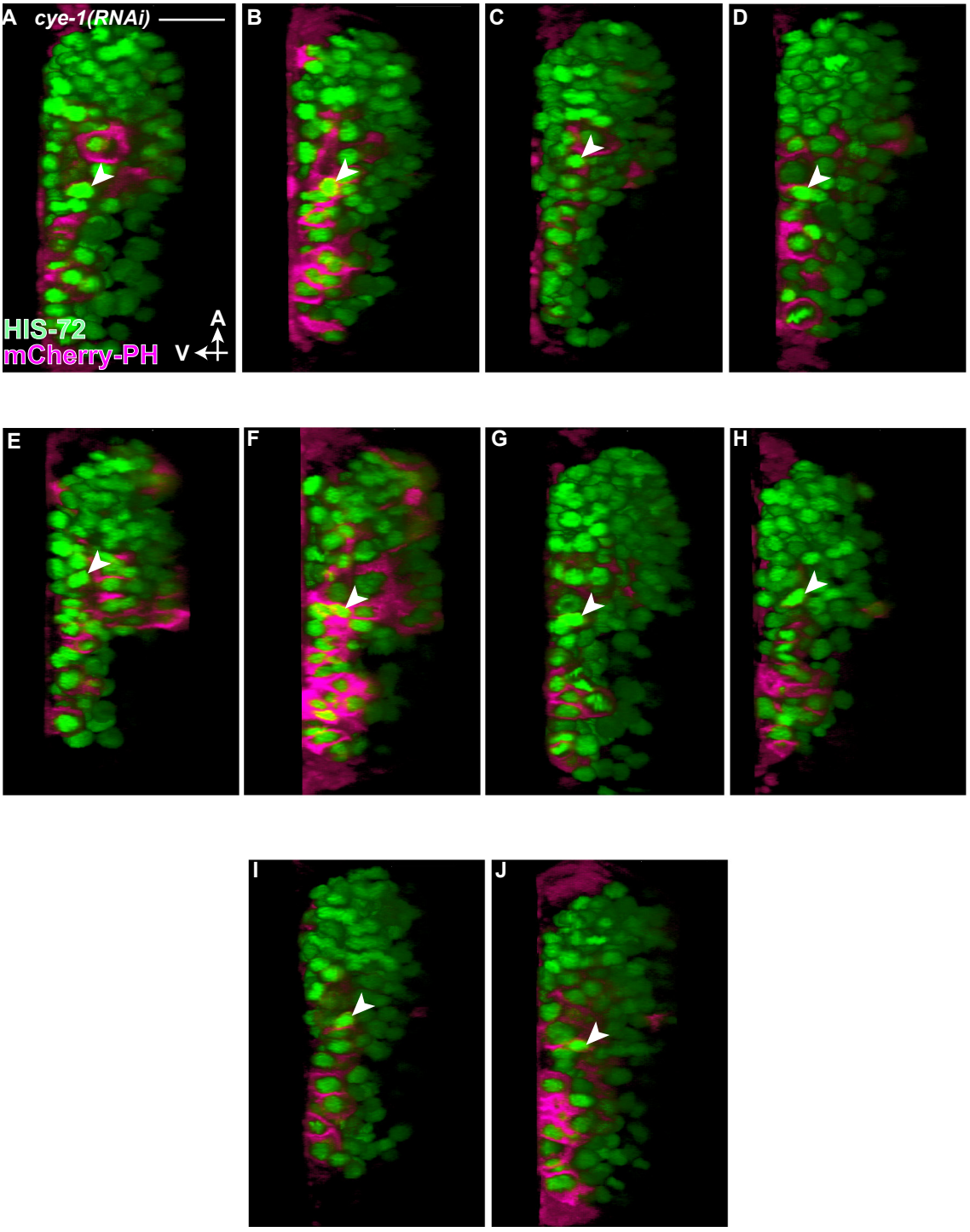

672 **Supplemental Figure 2 ABplpappap is not extruded by *cye-1(RNAi)***
673 **embryos**

674 (A-J) Virtual lateral sections of embryos through the ABplpappap cell (arrowhead)
675 in (A-J) 10 *cye-1(RNAi)* embryos show that ABplpappap is not extruded in 10 of
676 10 embryos. The embryos shown carry the transgenes *stIs10026* and *nIs861*. A,
677 anterior; V, ventral. Scale bar, 10 μm.

678

Supplemental Figure 3

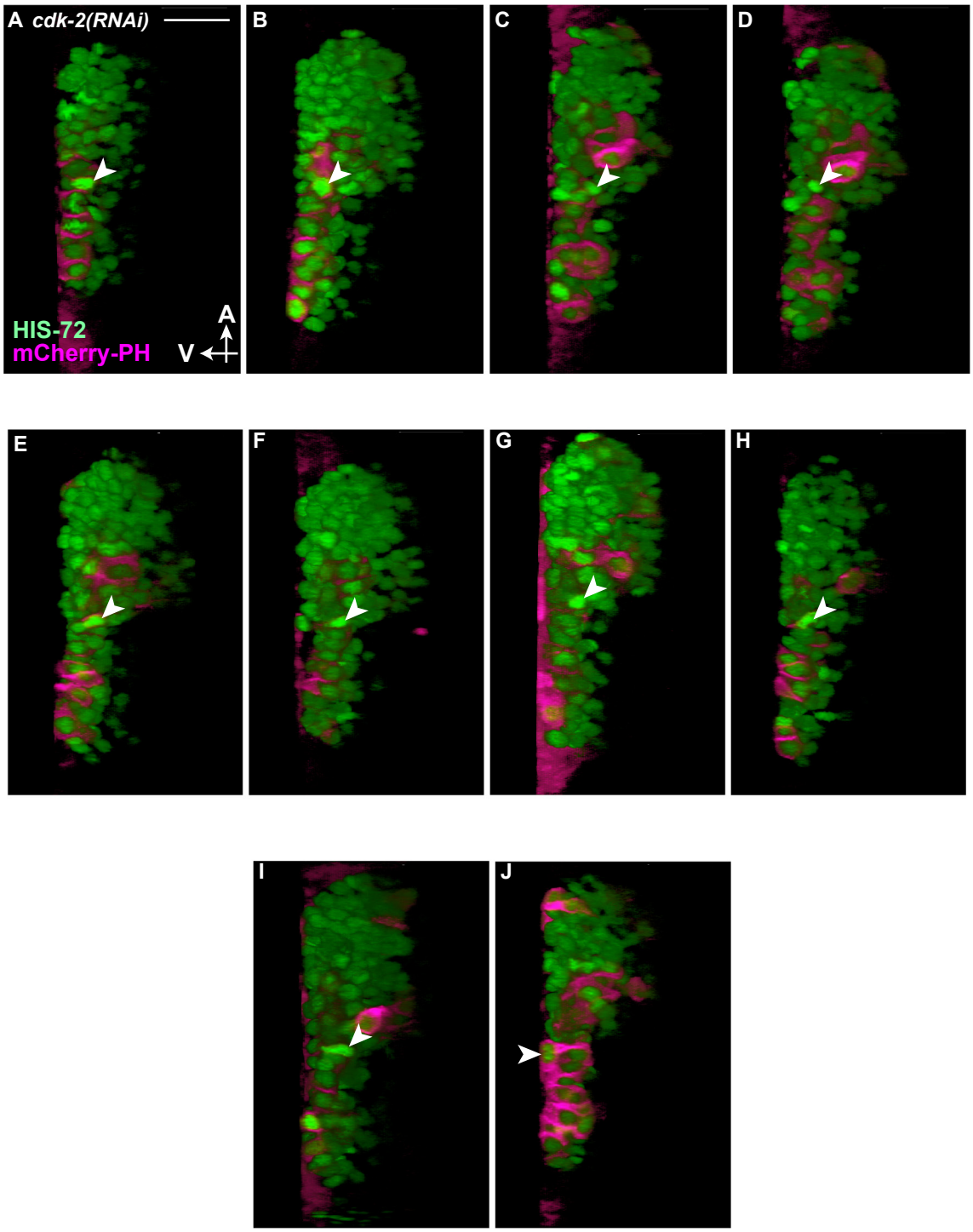

679 **Supplemental Figure 3 ABplpappap is not extruded by *cdk-2(RNAi)***
680 **embryos**

681 (A-J) Virtual lateral sections of embryos through the ABplpappap cell (arrowhead)
682 in (A-J) 10 *cdk-2(RNAi)* embryos show that (A-I) ABplpappap is not extruded in 9
683 of 10 embryos and (J) is extruded in 1 of 10 embryos. The embryos shown carry
684 the transgenes *stIs10026* and *nIs861*. A, anterior; V, ventral. Scale bar, 10 μm.
685

Supplemental Figure 4

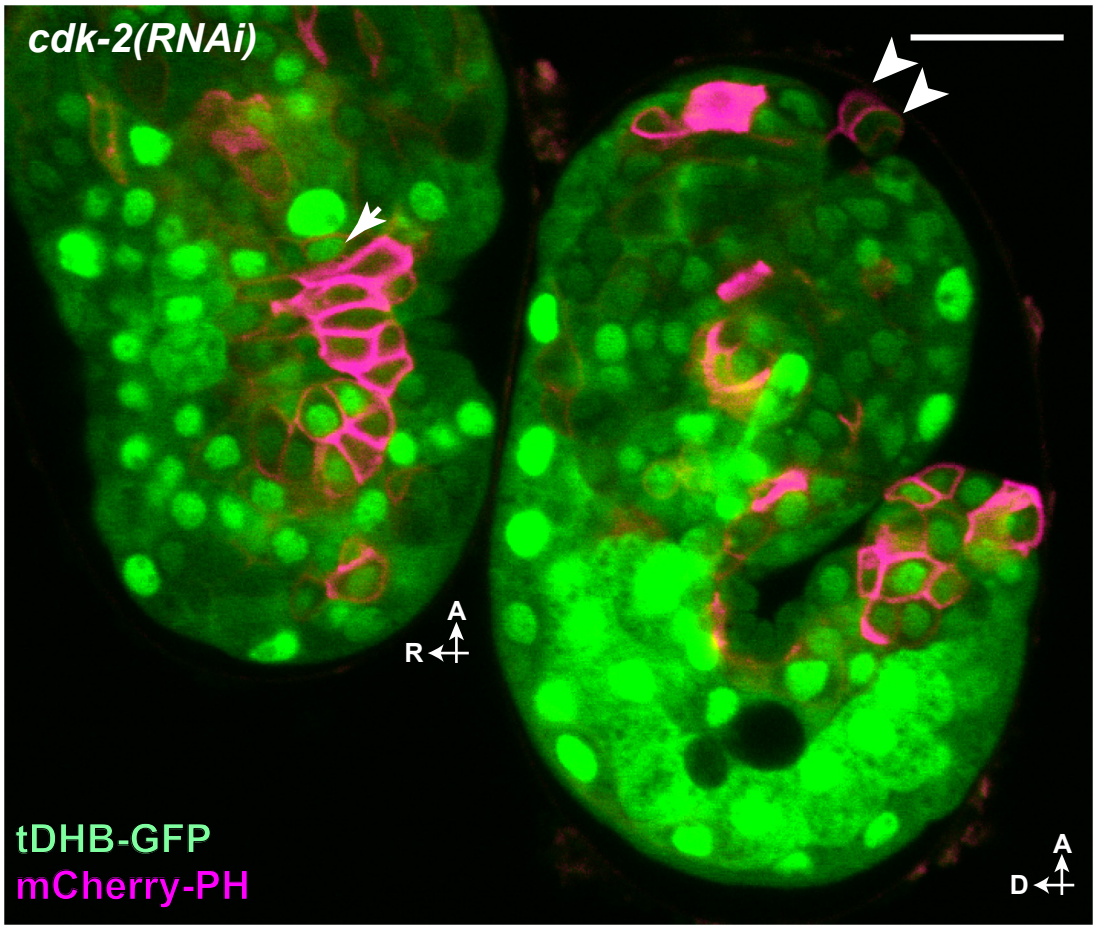

686 **Supplemental Figure 4 Cells extruded by *cdk-2(RNAi)* embryos enter the**
687 **cell cycle**

688 Micrograph of two *cdk-2(RNAi)* embryos expressing tDHB-GFP shows a nuclear-
689 enriched localization of tDHB-GFP in an ABplpappap cell (arrow) that was not
690 extruded by the first embryo but presumably nuclear-depleted tDHB-GFP in two
691 cells that were extruded from the second embryo (arrowheads). The embryos
692 shown carry the transgenes *heSi192* and *nIs861*. A, anterior; D, dorsal; R, right.
693 Scale bar, 10 μm.

694

Supplemental Figure 5

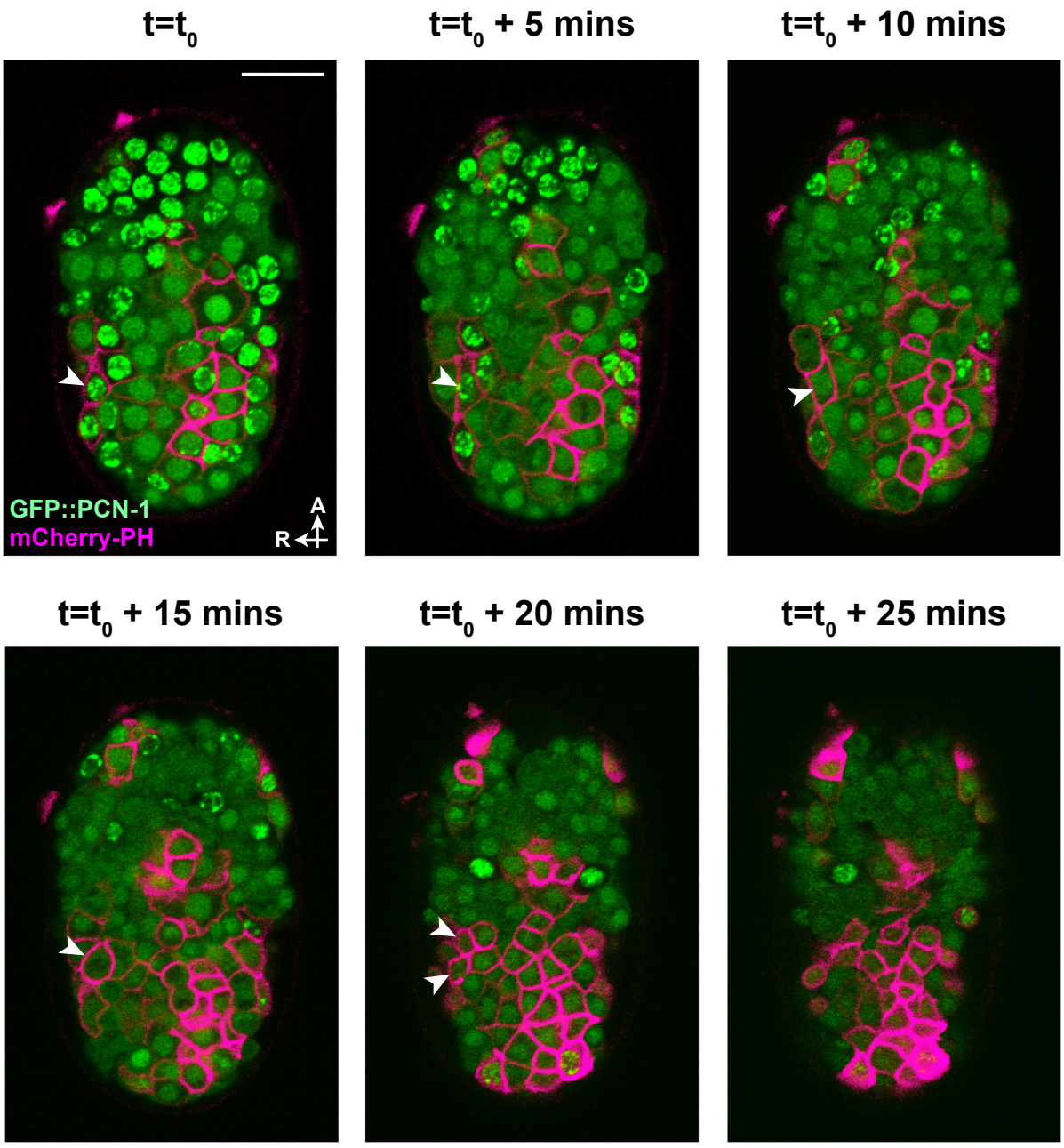

Supplemental Figure 5 GFP::PCN-1 exhibits a localization pattern coordinated with the cell cycle in embryonic cells on the ventral surface

Time-lapse confocal micrographs of a *ced-3(lf)* embryo obtained at 5-min intervals show the dynamics of GFP::PCN-1 localization in multiple cells on the ventral surface of the embryo. Arrowheads mark a cell that is shown undergoing a complete cell cycle. The embryo shown carries the transgenes *isIs17* and *nIs861*. A, anterior; R, right. Scale bar, 10 μm.

Supplemental Figure 6

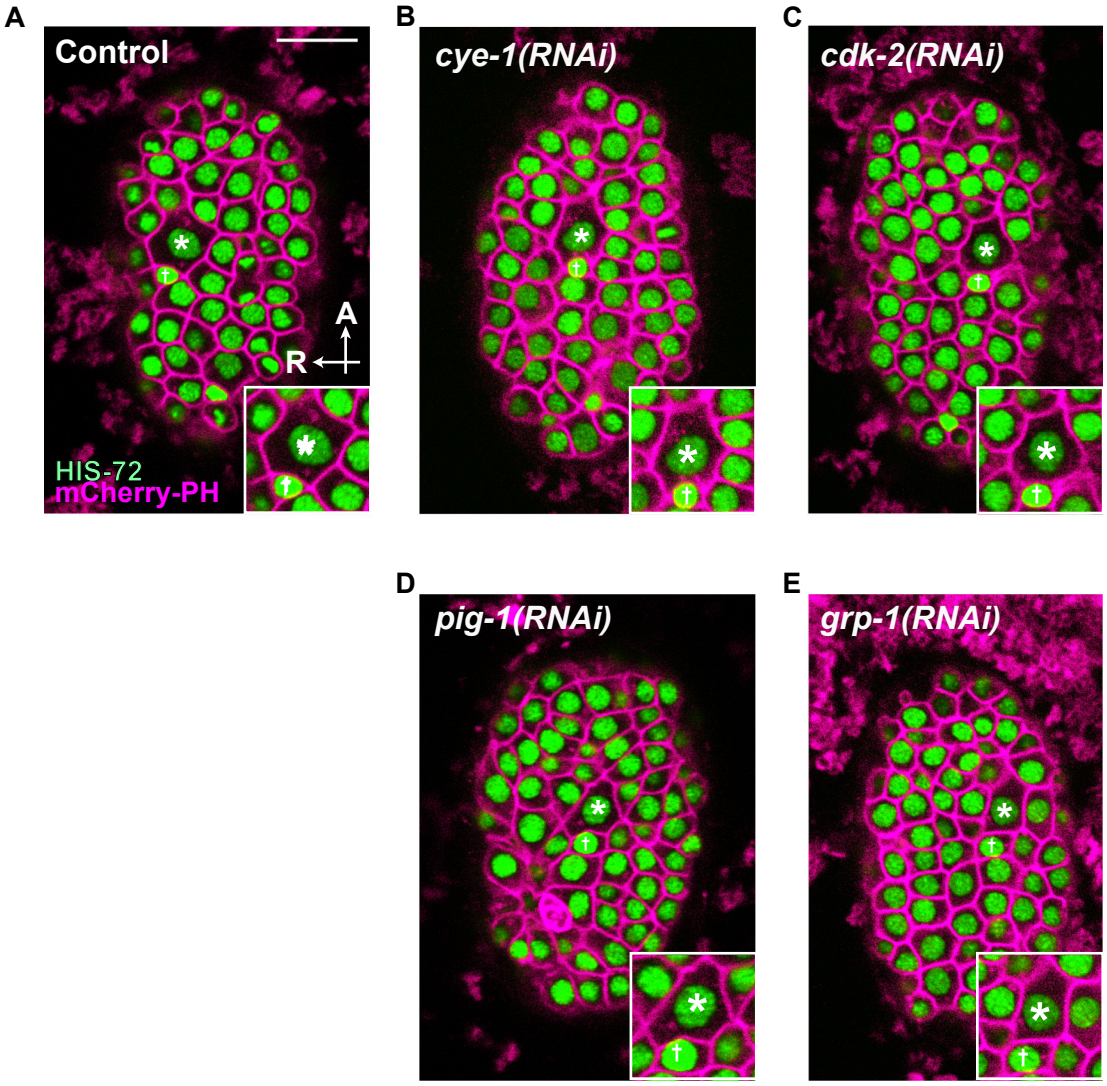

Supplemental Figure 6 ABplpappa undergoes unequal cell division controlled by *pig-1* and *grp-1* but independent of *cye-1* and *cdk-2*

Micrographs of *ced-3(lf)* embryos expressing nuclear GFP and membrane-localized mCherry in all cells obtained using confocal microscopy show the relative sizes of ABplpappap (†) and its sister, ABplpappaa (*) in a (A) control embryo, (B) *cye-1(RNAi)* embryo, (C) *cdk-2(RNAi)* embryo, (D) *pig-1(RNAi)* embryo and (E) *grp-1(RNAi)* embryo. Inset, a magnified view of ABplpappap(†) and its sister, ABplpappaa(*). All embryos shown carried the transgenes *stIs10026* and *ltIs44[$P_{pie\text{-}1}$::mCherry::PH]*, which expresses membrane-localized mCherry in all cells. A, anterior; R, right. Scale bar, 10 µm.

Supplemental Movies

Movie 1 Control embryos extrude ABplpappap as it undergoes ventral enclosure

Time-lapse video of a *ced-3(lf); control(RNAi)* embryo undergoing ventral enclosure over a period of 50 minutes shows ABplpappap (circled at the beginning and end of video) was extruded from this embryo. All nuclei are labeled with GFP and membranes of *egl-1*–expressing cells are labeled with mCherry (magenta). Time-lapse images used for this video were obtained using confocal microcopy. Video playback is at 600x real speed. The embryo shown carried the transgenes *stIs10026* and *nIs632*.

Movie 2 *cye-1(RNAi)* embryos do not extrude ABplpappap as it undergoes ventral enclosure

Time-lapse video of a *ced-3(lf); cye-1(RNAi)* embryo undergoing ventral enclosure over a period of 50 minutes shows ABplpappap (circled at the beginning and end of video) was not extruded from this embryo. All nuclei are labeled with GFP and membranes of *egl-1*–expressing cells are labeled with mCherry (magenta). Time-lapse images used for this video were obtained using confocal microcopy. Video playback is at 600x real speed. The embryo shown carried the transgenes *stIs10026* and *nIs632*.

Movie 3 *cdk-2(RNAi)* embryos do not extrude ABplpappap as it undergoes ventral enclosure

Time-lapse video of a *ced-3(lf); cdk-2 (RNAi)* embryo undergoing ventral enclosure over a period of 50 minutes shows ABplpappap (circled at the

beginning and end of video) was not extruded from this embryo. All nuclei are labeled with GFP and membranes of *egl-1*–expressing cells are labeled with mCherry (magenta). Time-lapse images used for this video were obtained using confocal microcopy. Video playback is at 600x real speed. The embryo shown carried the transgenes *stIs10026* and *nIs632*.

Movie 4 GFP::PCN-1 shows continuous change in fluorescence intensity during embryonic cell cycles

Time-lapse video of a *ced-3(lf)* embryo expressing GFP::PCN-1 in all cells shows continuous change in GFP::PCN-1 fluorescence intensity as cells progress through the cell cycle, similar to that observed for early embryonic cell cycles (Brauchle *et al*., 2003). Membranes of *egl-1*–expressing cells are labeled with mCherry (magenta). Time-lapse images used for this video were obtained using confocal microcopy. Video playback is at 180x real speed. The embryo shown carried the transgenes *isIs17* and *nIs861*.

Movie 5 ABplpappap divides before ventral enclosure and is not extruded in *pig-1(RNAi)* embryos

Time-lapse video of a *ced-3(lf); pig-1 (RNAi)* embryo undergoing ventral enclosure over a period of 57 minutes shows ABplpappap (circled at the beginning) divided to generate daughters (circled at the end of video) before ventral enclosure was complete in this embryo. All nuclei are labeled with GFP and membranes of *egl-1*–expressing cells are labeled with mCherry (magenta). Time-lapse images used for this video were obtained using confocal microcopy.

760 Video playback is at 600x real speed. The embryo shown carried the transgenes
761 *stIs10026* and *nIs861*.

762 **Movie 6 A few cells are extruded from a vehicle-treated MDCK monolayer**

763 A time-lapse video of mammalian MDCK monolayer treated with vehicle control
764 for 21.25 h shows that a few cells are extruded during this period. Extruded cells
765 can be identified as bright, white, rounded spots rising from the epithelial plane.
766 Video playback is at 7200x real speed. Scale bar, 100 μm.

767 **Movie 7 A large number of cells are extruded from an HU-treated MDCK**
768 **monolayer**

769 A time-lapse video of mammalian MDCK monolayer exposed to HU for 21.25 h
770 shows that many more cells are extruded during this period as a result of HU
771 treatment. Extruded cells can be identified as bright, white, rounded spots rising
772 from the epithelial plane. Video playback is at 7200x real speed. Scale bar, 100
773 μm.

KEY RESOURCES TABLE

REAGENT or RESOURCE	SOURCE	IDENTIFIER
Antibodies		
Bacterial and Virus Strains		
C. elegans and *E. coli* strains	This paper	Table S4
Biological Samples		
Chemicals, Peptides, and Recombinant Proteins		
Chemical: Isopropyl-β-D-thiogalactopyranoside	Amresco	Cat#0487
Chemical: Hydroxyurea	Millipore Sigma	Cat#H8627
Critical Commercial Assays		
In-Fusion HD Cloning Assays	TaKaRa	Cat#639637
QuikChange Site-Directed Mutagenesis Kit	Agilent	Cat#200515
Phusion High-Fidelity DNA Polymerase	New England Biolabs	Cat#M0530L
Q5 Hot Start High-Fidelity DNA Polymerase	New England Biolabs	Cat#M0439L
Deposited Data		
Experimental Models: Cell Lines		
Experimental Models: Organisms/Strains		
C. elegans and *E. coli* strains	This Paper	Table S4
Oligonucleotides		
Forward primer to amplify *egl-1* promoter: CGCctgcagTTGAAATTTGGGGATATTTTGG	This Paper	DPD660
Reverse primer to amplify *egl-1* promoter: CGCgagctcCTGGAAATTAGTAAGGTTTTGAAGGGGG	This Paper	DPD661
Forward primer to amplify mCherry PLC-1δ PH domain: CGCaccggtCCAGATGGCTCAAACAAAGC	This Paper	DPD647
Reverse primer to amplify mCherry PLC-1δ PH domain: CGCgaattcGGCACAAGTTCATTCACAGG	This Paper	DPD648
Forward primer to remove NLS sequence: ggagctcAGAAAAAATGGTCTCAAAGGGTG	This Paper	DPD695
Reverse primer to remove NLS sequence: CACCCTTTGAGACCATTTTTTCTgagctcc	This Paper	DPD696
Forward primer to amplify *atl-1* genomic region for RNAi: TCGAATTCCTGCAGCTCCTCGAACCCATCATCCCT	This Paper	RD105
Reverse primer to amplify *atl-1* genomic region for RNAi: TGACGCGTGGATCCCATGAAGCTGCGTGGTTGTTG	This Paper	RD106
Forward primer to amplify *mat-2* genomic region for RNAi: TCGAATTCCTGCAGCCTGGAACTCATCCCATACGC	This Paper	RD103
Reverse primer to amplify *mat-2* genomic region for RNAi: TGACGCGTGGATCCCCATTGGAACCTCCAGATGCT	This Paper	RD104
Additional oligonucleotides	This Paper	Table S3
Recombinant DNA		
pDD111 – P_{egl-1}*::mCherry::PH::unc-54 3'UTR*	This Paper	N/A
pL4440 – *atl-1*	This Paper	N/A

pL4440 – *mat-2*	This Paper	N/A
pL4440 – *lin-15B*	This Paper	N/A
pAA173	Ziel *et al*., 2009	N/A
pPD122.56	Andrew Fire	L4054, RRID:Addgene_1632
p76-16B	Bloom and Horvitz, 1997	N/A
pML902	McMahon *et al*., 2001	N/A
Software and Algorithms		
ImageJ	NIH	https://imagej.nih.gov/ij/
GraphPad Prism 7	GraphPad Software	https://www.graphpad.com/scientific-software/prism/
Zen Blue	Zeiss	https://www.zeiss.com/microscopy/us/downloads/zen.html
Adobe Photoshop and Illustrator	Adobe	https://www.adobe.com/creativecloud.html
Geneious 10.2.6	Biomatters, Inc.	https://www.geneious.com/
Stowers ImageJ Plugin	Jay Unruh	https://research.stowers.org/imagejplugins/index.html
Other		

Table S3. Additional Oligonucleotides.

REAGENT OR RESOURCE	SOURCE	IDENTIFIER
Forward primer to amplify *lin-15B* genomic DNA for RNAi: TCGAATTCCTGCAGCGCTGACACAATTGCGAACAT	This paper	RD101
Reverse primer to amplify *lin-15B* genomic DNA for RNAi: TGACGCGTGGATCCCCGTGTGCATAAAGACCAAGG	This paper	RD102

Table S4. *C. elegans* and *E. coli* strains.

REAGENT OR RESOURCE	SOURCE	IDENTIFIER
C. elegans Strain: Bristol N2	*Caenorhabditis* Genetics Center	N2
C. elegans Strain OD70: *unc-119(ed3)* III; *ltIs44* V	*Caenorhabditis* Genetics Center, Kachur *et al.*, (2008)	OD70; RRID:WB-STRAIN:OD70
C. elegans Strain GZ264: *unc-119(ed3)* III; *isIs17*	*Caenorhabditis* Genetics Center, Brauchle *et al.* (2003)	GZ264; RRID:WB-STRAIN:GZ264
C. elegans Strain SV1668: *heSi192* II; *unc-119(ed3)* III	van Rijnberk *et al.* (2017)	N/A
C. elegans Strain RW10026: *stIs10026*	*Caenorhabditis* Genetics Center, Boeck *et al.*, (2011)	RW10026; RRID:WB-STRAIN:RW10026
C. elegans Strain MT8034: *ced-3(n717)* IV; *unc-76(e911)* V	This paper	N/A
C. elegans Strain MT12054: *ced-3(n3692)* IV	Denning *et al.* (2012)	N/A
C. elegans Strain MT20083: *nIs433* I	Denning *et al.* (2012)	N/A
C. elegans Strain MT20117: *nIs433* I; *ced-3(n3692)* IV	Denning *et al.* (2012)	N/A
C. elegans Strain MT22348: *ced-3(n717)* IV; *unc-76(e911)* V; *nEx2188*	This paper	N/A
C. elegans Strain MT22380: *ced-3(n717)* IV; *unc-76(e911)* V; *nIs632*	This paper	N/A
C. elegans Strain MT22450: *ced-3(n3692)* IV; *stIs10026*; *nIs632*	This paper	N/A
C. elegans Strain MT25568: *ced-3(n3692)* IV; *nIs861*	This paper	N/A
C. elegans Strain MT25639: *ced-3(n3692)* IV; *stIs10026*; *nIs861*	This paper	N/A
C. elegans Strain MT25640: *heSi192* II; *ced-3(n3692)* IV; *nIs861*	This paper	N/A
C. elegans Strain MT25692: *ced-3(n3692)* IV; *ltIs44* V; *stIs10026*	This paper	N/A
C. elegans Strain MT25807: *ced-3(n3692)* IV; *nIs861*; *isIs17*	This paper	N/A

REAGENT OR RESOURCE	SOURCE	IDENTIFIER
Escherichia coli: OP50	*Caenorhabditis* Genetics Center	WB Cat#OP50, RRID:WB-STRAIN:OP50
Escherichia coli: HT115	*Caenorhabditis* Genetics Center	WB Cat#HT115, RRID:WB-STRAIN:HT115
Escherichia coli: HT115-pL4440 (Control)	Timmons and Fire, (1998)	
Escherichia coli: HT115-*W03G6.1* (*pig-1*)	Fraser *et al.* (2000), Source BioScience	Cat#3318_Cel_RNAi_complete
Escherichia coli: HT115-*C17G10.4* (*cdc-14*)	Fraser *et al.* (2000), Source BioScience	Cat#3318_Cel_RNAi_complete
Escherichia coli: HT115-*K06A5.7* (*cdc-25.1*)	Fraser *et al.* (2000), Source BioScience	Cat#3318_Cel_RNAi_complete
Escherichia coli: HT115-*F16B4.8* (*cdc-25.2*)	Fraser *et al.* (2000), Source BioScience	Cat#3318_Cel_RNAi_complete
Escherichia coli: HT115-*ZK637.11* (*cdc-25.3*)	Fraser *et al.* (2000), Source BioScience	Cat#3318_Cel_RNAi_complete
Escherichia coli: HT115-*R05H5.2* (*cdc-25.4*)	Fraser *et al.* (2000), Source BioScience	Cat#3318_Cel_RNAi_complete
Escherichia coli: HT115-*T05G5.3* (*cdk-1*)	Rual *et al.*, (2004), Open BioSystems	Cat#RCE1182
Escherichia coli: HT115-*B0495.2* (*cdk-11.1*)	Fraser *et al.* (2000), Source BioScience	Cat#3318_Cel_RNAi_complete
Escherichia coli: HT115-*ZC504.3* (*cdk-11.2*)	Fraser *et al.* (2000), Source BioScience	Cat#3318_Cel_RNAi_complete
Escherichia coli: HT115-*B0285.1* (*cdk-12*)	Rual *et al.*, (2004), Open BioSystems	Cat#RCE1182
Escherichia coli: HT115-*K03E5.3* (*cdk-2*)	Fraser *et al.* (2000), Source BioScience	Cat#3318_Cel_RNAi_complete
Escherichia coli: HT115-*F18H3.5* (*cdk-4*)	Fraser *et al.* (2000), Source BioScience	Cat#3318_Cel_RNAi_complete
Escherichia coli: HT115-*T27E9.3* (*cdk-5*)	Fraser *et al.* (2000), Source BioScience	Cat#3318_Cel_RNAi_complete
Escherichia coli: HT115-*Y39G10AL.3* (*cdk-7*)	Rual *et al.*, (2004), Open BioSystems	Cat#RCE1182
Escherichia coli: HT115-*F39H11.3* (*cdk-8*)	Fraser *et al.* (2000), Source BioScience	Cat#3318_Cel_RNAi_complete
Escherichia coli: HT115-*H25P06.2* (*cdk-9*)	Fraser *et al.* (2000), Source BioScience	Cat#3318_Cel_RNAi_complete
Escherichia coli: HT115-*Y54E10A.15* (*cdt-1*)	Rual *et al.*, (2004), Open BioSystems	Cat#RCE1182
Escherichia coli: HT115-*Y39H10A.7* (*chk-1*)	Rual *et al.*, (2004), Open BioSystems	Cat#RCE1182
Escherichia coli: HT115-*F44B9.4* (*cit-1.1*)	Source BioScience	Cat#3317_Cel_RNAi_supplement_whole
Escherichia coli: HT115-*F44B9.3* (*cit-1.2*)	Fraser *et al.* (2000), Source BioScience	Cat#3318_Cel_RNAi_complete
Escherichia coli: HT115-*T05A6.1* (*cki-1*)	Fraser *et al.* (2000), Source BioScience	Cat#3318_Cel_RNAi_complete
Escherichia coli: HT115-*T05A6.2* (*cki-2*)	Fraser *et al.* (2000), Source BioScience	Cat#3318_Cel_RNAi_complete
Escherichia coli: HT115-*C07H6.6* (*clk-2*)	Source BioScience	Cat#3317_Cel_RNAi_supplement_whole
Escherichia coli: HT115-*D2045.6* (*cul-1*)	Fraser *et al.* (2000), Source BioScience	Cat#3318_Cel_RNAi_complete
Escherichia coli: HT115-*ZK520.4 (cul-2)*	Rual *et al.*, (2004), Open BioSystems	Cat#RCE1182

Escherichia coli: HT115-*Y108G3AL.1 (cul-3)*	Source BioScience	Cat#3317_Cel_RNAi_supplement_whole
Escherichia coli: HT115-*F45E12.3* (*cul-4*)	Fraser *et al.* (2000), Source BioScience	Cat#3318_Cel_RNAi_complete
Escherichia coli: HT115-*ZK507.6* (*cya-1*)	Rual *et al.*, (2004), Open BioSystems	Cat#RCE1182
Escherichia coli: HT115-*ZC168.4* (*cyb-1*)	Source BioScience	Cat#3317_Cel_RNAi_supplement_whole
Escherichia coli: HT115-*Y43E12A.1* (*cyb-2.1*)	Rual *et al.*, (2004), Open BioSystems	Cat#RCE1182
Escherichia coli: HT115-*H31G24.4* (*cyb-2.2*)	Rual *et al.*, (2004), Open BioSystems	Cat#RCE1182
Escherichia coli: HT115-*T06E6.2* (*cyb-3*)	Fraser *et al.* (2000), Source BioScience	Cat#3318_Cel_RNAi_complete
Escherichia coli: HT115-*H14E04.5* (*cic-1*)	Source BioScience	Cat#3317_Cel_RNAi_supplement_whole
Escherichia coli: HT115-*Y38F1A.5* (*cyd-1*)	Fraser et al. (2000), Source BioScience	Cat#3318_Cel_RNAi_complete
Escherichia coli: HT115-*C37A2.4* (*cye-1*)	Rual *et al.*, (2004), Open BioSystems	Cat#RCE1182
Escherichia coli: HT115-*Y49F6B.1* (*cyh-1*)	Rual *et al.*, (2004), Open BioSystems	Cat#RCE1182
Escherichia coli: HT115-*C52E4.6* (*cyl-1*)	Fraser et al. (2000), Source BioScience	Cat#3318_Cel_RNAi_complete
Escherichia coli: HT115-*ZK353.1* (*cyy-1*)	Fraser et al. (2000), Source BioScience	Cat#3318_Cel_RNAi_complete
Escherichia coli: HT115-*T23G7.1* (*dpl-1*)	Source BioScience	Cat#3317_Cel_RNAi_supplement_whole
Escherichia coli: HT115-*Y102A5C.18* (*efl-1*)	Fraser et al. (2000), Source BioScience	Cat#3318_Cel_RNAi_complete
Escherichia coli: HT115-*F10B5.6* (*emb-27*)	Fraser et al. (2000), Source BioScience	Cat#3318_Cel_RNAi_complete
Escherichia coli: HT115-*F54C8.3* (*emb-30*)	Fraser et al. (2000), Source BioScience	Cat#3318_Cel_RNAi_complete
Escherichia coli: HT115-*ZK1307.6* (*fzr-1*)	Source BioScience	Cat#3317_Cel_RNAi_supplement_whole
Escherichia coli: HT115-*ZK177.6* (*fzy-1*)	Fraser et al. (2000), Source BioScience	Cat#3318_Cel_RNAi_complete
Escherichia coli: HT115-*F32A11.2* (*hpr-17*)	Fraser et al. (2000), Source BioScience	Cat#3318_Cel_RNAi_complete
Escherichia coli: HT115-*H26D21.1* (*hus-1*)	Fraser et al. (2000), Source BioScience	Cat#3318_Cel_RNAi_complete
Escherichia coli: HT115-*K10B2.1* (*lin-23*)	Fraser et al. (2000), Source BioScience	Cat#3318_Cel_RNAi_complete
Escherichia coli: HT115-*C32F10.2* (*lin-35*)	Fraser et al. (2000), Source BioScience	Cat#3318_Cel_RNAi_complete
Escherichia coli: HT115-*F44B9.6* (*lin-36*)	Fraser et al. (2000), Source BioScience	Cat#3318_Cel_RNAi_complete
Escherichia coli: HT115-*ZK637.7* (*lin-9*)	Fraser et al. (2000), Source BioScience	Cat#3318_Cel_RNAi_complete
Escherichia coli: HT115-*Y110A7A.17* (*mat-1*)	Rual *et al.*, (2004), Open BioSystems	Cat#RCE1182
Escherichia coli: HT115-*F10C5.1* (*mat-3*)	Rual *et al.*, (2004), Open BioSystems	Cat#RCE1182
Escherichia coli: HT115-*C50F4.11* (*mdf-1*)	Rual *et al.*, (2004), Open BioSystems	Cat#RCE1182
Escherichia coli: HT115-*Y69A2AR.30* (*mdf-2*)	Rual *et al.*, (2004), Open BioSystems	Cat#RCE1182

Escherichia coli: HT115-*Y41C4A.14* (*mrt-2*)	Rual *et al*., (2004), Open BioSystems	Cat#RCE1182
Escherichia coli: HT115-*T23G5.1* (*rnr-1*)	Rual *et al*., (2004), Open BioSystems	Cat#RCE1182
Escherichia coli: HT115-*ZC328.4* (*san-1*)	Rual *et al*., (2004), Open BioSystems	Cat#RCE1182
Escherichia coli: HT115-*F35H8.7* (*wee-1.1*)	Rual *et al*., (2004), Open BioSystems	Cat#RCE1182
Escherichia coli: HT115-*Y53C12A.1* (*wee-1.3*)	Rual *et al*., (2004), Open BioSystems	Cat#RCE1182
Escherichia coli: HT115- *R53.6* (*psf-1*)	Rual *et al*., (2004), Open BioSystems	Cat#RCE1182
Escherichia coli: HT115-*F31C3.5* (*psf-2*)	Rual *et al*., (2004), Open BioSystems	Cat#RCE1182
Escherichia coli: HT115-*Y65B4BR.8* (*psf-3*)	Rual *et al*., (2004), Open BioSystems	Cat#RCE1182
Escherichia coli: HT115-*Y59A8A.1* (*csn-1*)	Rual *et al*., (2004), Open BioSystems	Cat#RCE1182
Escherichia coli: HT115-*Y55F3AM.15* (*csn-4*)	Rual *et al*., (2004), Open BioSystems	Cat#RCE1182
Escherichia coli: HT115-*B0547.1* (*csn-5*)	Rual *et al*., (2004), Open BioSystems	Cat#RCE1182
Escherichia coli: HT115-*Y39A1A.23* (*hpr-9*)	Source BioScience	Cat#3317_Cel_RNAi_supplement_whole
Escherichia coli: HT115-*Y75B8A.22* (*tim-1*)	Source BioScience	Cat#3317_Cel_RNAi_supplement_whole
Escherichia coli: HT115-*F23C8.9* (*tipn-1*)	Fraser et al. (2000), Source BioScience	Cat#3318_Cel_RNAi_complete
Escherichia coli: HT115-*F37D6.1* (*mus-101*)	Fraser et al. (2000), Source BioScience	Cat#3318_Cel_RNAi_complete
Escherichia coli: HT115-*F25H5.5* (*clsp-1*)	Fraser et al. (2000), Source BioScience	Cat#3318_Cel_RNAi_complete
Escherichia coli: HT115-*F18A1.5* (*rpa-1*)	Fraser et al. (2000), Source BioScience	Cat#3318_Cel_RNAi_complete
Escherichia coli: HT115-*T06E4.3* (*atl-1*)	This paper	N/A
Escherichia coli: HT115-*W10C6.1* (*mat-2*)	This paper	N/A
Escherichia coli: HT115-*ZK662.4* (*lin-15B*)	This paper	N/A
C. elegans ORFeome RNAi Library v1.1	Rual *et al*., (2004), Open BioSystems	Cat#RCE1182

Materials and Methods

Plasmids

L4054 was a gift from Andrew Fire (Addgene plasmid # 1632; http://n2t.net/addgene:1632 ; RRID:Addgene_1632). pDD111 - *P_{egl-1}::mCherry::PH::unc-54 3'UTR* was generated with the following steps: i) 6.8 Kb of the *egl-1* promoter was amplified from genomic DNA with Phusion DNA polymerase using the primers DPD660 and DPD661; ii) the amplicon was digested with PstI and SacI (New England Biolabs) and ligated into pPD122.56, which encodes 4xNLS::GFP to generate *P_{egl-1}::4xNLS::GFP::unc-54 3'UTR*; iii) mCherry-PH (Pleckstrin Homology) sequence was amplified from pAA173 using DPD647 and DPD648 and digested with EcoRI and AgeI (New England Biolabs) and ligated into the pDD122.56 - *P_{egl-1}::4xNLS::GFP::unc-54 3'UTR*, which generated the plasmid pDD122.56 - *P_{egl-1}::4xNLS::mCherry::PH::unc-54 3'UTR*; iv) the 4xNLS sequence was removed with the primers DPD695 and DPD696 using QuikChange Site-Directed Mutagenesis (Agilent) to generate pDD111 - *P_{egl-1}::mCherry::PH::unc-54 3'UTR*.

RNAi clones were constructed for *atl-1*, *mat-2* and *lin-15B*. Genomic regions of about 1 kb were amplified from wild-type genomic lysates using Q5 Hot Start high-fidelity polymerase (New England Biolabs) with the following primers:

atl-1

RD105 TCGAATTCCTGCAGCTCCTCGAACCCATCATCCCT

RD106 TGACGCGTGGATCCCATGAAGCTGCGTGGTTGTTG

mat-2

RD103 TCGAATTCCTGCAGCCTGGAACTCATCCCATACGC

RD104 TGACGCGTGGATCCCCATTGGAACCTCCAGATGCT

lin-15B

RD101 TCGAATTCCTGCAGCGCTGACACAATTGCGAACAT

RD102 TGACGCGTGGATCCCCGTGTGCATAAAGACCAAGG

These inserts were cloned into the pL4440 vector linearized with *XmaI* (New England Biolabs) using the In-Fusion HD cloning kit (TaKaRa) according to manufacturers instructions. The cloned vector was then transformed into competent HT115 bacterial cells. Correct RNAi clones were identified by Sanger sequencing. Geneious 10.2.6 (Biomatters, Inc.) was used to guide all plasmid design and construction.

Contact for Reagent and Resource Sharing

Further information and resource sharing requests should be directed to and will be fulfilled by the lead contact, H. Robert Horvitz (horvitz@mit.edu).

Strains, transgenes and mutations

C. elegans hermaphrodite strains were maintained on Nematode Growth Medium (NGM) plates containing 3 g/L NaCl, 2.5 g/L peptone and 17 g/L agar supplemented with 1 mM $CaCl_2$, 1 mM $MgSO_4$, 1 mM KPO_4 and 5 mg/L Cholesterol with E. coli OP50 as a source of food (Brenner, 1974). All strains were derived from Bristol N2 and are listed in Table S2. *ced-3(lf)* refers to the *n3692* deletion allele of *ced-3* (Denning *et al*., 2012). *C. elegans* strains carrying the transgenes *nIs861* and *isIs17* were maintained at 25°C. All other strains were maintained at 22°C. The transgenes and mutations used are listed below:

LGI: *nIs433[P_{pgp-12}::4xNLS::GFP::unc-54 3'UTR; p76-16B(unc-76(+))]*

LGII: *heSi192[P_{eft-3}::tDHB::eGFP::tbb-2 3'UTR + Cbr-unc119(+)]*

LGIII: *unc-119(ed3)*

LGIV: *ced-3(n3692, n717)*

LGV: *unc-76(e911)*, *ltIs44[P_{pie-1}::mCherry::PH(PLC1delta1) + unc-119(+)]*

Unknown linkage: *stIs10026[P_{his-72}::HIS-72::GFP]*, *isIs17[pGZ295(P_{pie-1}::GFP::pcn-1(W03D2.4)), pDP#MM051 (unc-119(+))]*, *nIs861[pDD111(P_{egl-1}::mCherry::PH::unc-54 3'UTR)]*, *nIs632[pDD111(P_{egl-1}::mCherry::PH::unc-54 3'UTR), pML902 (dlg-1::GFP),p76-16B(unc-76(+))]*

Extrachromosomal array: *nEx2188[pDD111(P_{egl-1}::mCherry::PH::unc-54 3'UTR), pML902 (dlg-1::GFP), unc-76(+)]*

nIs632 and *nIs861* express membrane-localized mCherry from the *egl-1* promoter, which facilitated the identification of ABplpappap (an *egl-1* expressing cell). *nIs632* does not express *dlg-1::GFP*, presumably as a result of partial transgene silencing (Hsieh *et al*. 1999; Grishok *et al*. 2005; Fischer *et al*. 2013). *stIs10026* (Boeck *et al*., 2011) ubiquitously expresses a GFP-tagged histone HIS-72 from its endogenous promoter, which produces fluorescence in the nuclei of all cells and facilitates in providing the context in which extrusion events are observed.

Germline transformation

Transgenic lines were generated using the standard germline transformation procedure (Mello *et al*., 1991). Extrachromosomal array transgene *nEx2188* was generated by injecting pML902 at 3 ng/µL, pDD111 at 40 ng/µL, p76-16B (unc-

844 76(+)) at 60 ng/ul and 1Kb Plus DNA ladder (Thermo Fischer Scientific) at 50 ng/
845 µl into *ced-3(n717) IV; unc-76(e911) V* double mutant animals. *nIs632* was
846 generated by gamma-ray irradiation (4,800 rads) of *nEx2188*-carrying L4 animals
847 and was identified by the 100% transmission of the transgene from transformed
848 parent to progeny. *nIs861* was a spontaneous integration in a germline cell of an
849 animal injected with pDD111 at 10 ng/µL and 1 kb DNA ladder at 90 ng/µL, and
850 was identified by the 100% transmission of the transgene from transformed
851 parent to progeny.

852 **RNAi treatments and genome-wide RNAi screen**

853 Previously described feeding RNAi constructs and reagents were used to
854 perform RNAi feeding experiments (Fraser *et al*., 2000; Rual *et al*., 2004). Briefly,
855 HT115 *Escherichia coli* bacteria carrying RNAi clones in the pL4440 vector were
856 grown for at least 12 h in Luria broth (LB) liquid media with 75 mg/L ampicillin at
857 37°C. These cultures were seeded onto 6 cm Petri plates with Nematode Growth
858 Medium (NGM) containing 1 mM isopropyl-β-D-thiogalactopyranoside (IPTG)
859 (Amresco) and 75 mg/L ampicillin and incubated for 24 h at 22°C. For imaging
860 experiments using confocal microscopy, 10 L4 animals were added to each RNAi
861 plate and imaging of progeny embryos was performed on the next day as
862 described in Microscopy below. For excretory cell counts, five L4 animals were
863 added to each RNAi plate and L3-L4 progeny were scored for number of
864 excretory cells, as described in Excretory cell count below. In case a bacterial
865 clone targeting a certain gene was not available in previously constructed

866 libraries (Kamath *et al*., 2003; Rual *et al*., 2004), we generated our own RNAi
867 clone as described in Molecular biology above.

868 The ORFeome RNAi library was used to conduct a genome-wide RNAi
869 screen (Rual *et al*., 2004). For each day of the RNAi screen, all bacterial colonies
870 from two 96-well plates were cultured for at least 12 h at 37°C in LB with 75 mg/L
871 ampicillin. These cultures were then pre-incubated with 1 mM IPTG (Amresco)
872 for 1 h to maximize induction of dsRNA production. 24-well plates with each well
873 containing 2 mL NGM medium with 1 mM IPTG (Amresco) and 75 mg/L
874 ampicillin were prepared in advance and stored at 4°C until needed; they were
875 brought to room temperature a few hours before seeding. Each bacterial colony
876 culture was then seeded onto an individual well of a 24-well plate and incubated
877 for 24 h at 20°C. Three L4 animals were picked into a 10 µl drop of M9 medium,
878 which facilitated their transfer into a well using a pipette. The progeny of these 3
879 animals were screened 3 days later. Each set of RNAi clones screened also
880 included a *pig-1* RNAi positive control and an empty pL4440 vector negative
881 control. The scorer was blinded to the identity of the RNAi clones. Excretory cell
882 counts were performed as described in Excretory cell counts below. Sanger
883 sequencing was used to confirm the identity of RNAi clones that reproducibly
884 generated a Tex phenotype for more than 10% of the animals scored.

885 **Microscopy**

886 All RNAi screens scoring excretory cells were performed using a Nikon SMZ18
887 fluorescent dissecting microscope. DIC and epifluorescence images were

obtained using a 63x objective lens (Zeiss) on an AxioImager Z2 (Zeiss) compound microscope and Zen Blue software (Zeiss).

For confocal microscopy, embryos staged at the 200-300-cell stage were picked and mounted onto a glass slide (Corning) with a freshly prepared 2% agarose pad. Embryos with ventral surfaces facing the objective were selected for imaging. Confocal images were obtained using a 63x objective lens (Zeiss) on a Zeiss LSM800 confocal microscope.

For observing extrusion (or absence of extrusion), we focused particularly on the cell ABplpappap, the identification of which is facilitated by its central position on the ventral surface (Sulston *et al*., 1983). The fluorescent transgene *nIs861[Pegl-1::mCherry::PH]* or *nIs632[Pegl-1::mCherry::PH; dlg-1::GFP]*, which express the Pleckstrin homology domain of PLC-δ fused to mCherry from the promoter of *egl-1*, was used to label the membrane of the ABplpappap cell, an *egl-1* expressing cell (Denning *et al*., 2012), to further facilitate cell identification. Another fluorescent transgene *stIs10026[his-72::GFP]*, which expresses GFP-tagged HIS-72 histone protein, was used to label the nuclei of all cells to help define ABplpappap's location within the embryo. Time-lapse confocal microscopy was used to monitor the location of ABplpappap in embryos, keeping the cell in view by refocusing on it every 30 sec. Confocal imaging during a period of about 50 min during which ventral enclosure (migration and meeting of hypodermal cells on the ventral surface of the embryo) occurs was sufficient to determine whether ABplpappap did or did not undergo extrusion.

For determining whether ABplpappap and other cells that are extruded entered the cell cycle, the transgene *heSi192[Peft-3::tDHB::eGFP::tbb-2 3'UTR]* was used to express a codon-optimized (for *C. elegans*) C-terminal fragment of Human DNA Helicase B, which translocates from the nucleus to the cytoplasm in response to the activity of the cell cycle CDKs 1 and 2 (van Rijnberk *et al*., 2017). *nIs861* was used to label the membrane of ABplpappap with mCherry to facilitate cell identification.

For determining the cell cycle phase of ABplpappap and other extruded cells, *isIs17[Ppie-1::GFP::PCN-1]* was used to express GFP-tagged PCN-1 protein, which produces a phase-specific fluorescence intensity and localization pattern. *nIs861* was used to label the membrane of ABplpappap with mCherry to facilitate cell identification.

Images were processed with ImageJ software (NIH), Photoshop CC 2019 (Adobe) and Illustrator CC 2019 (Adobe) software. The Time Stamper function in the Stowers ImageJ plugin was used to mark elapsed time on time-lapse videos.

Excretory cell counts

Excretory cell counts were performed using a dissecting microscope equipped with fluorescence at a total magnification of 270x. For the genome-wide RNAi screen, roughly 50 animals were examined in each well of a 24-well plate and any well with more than 5 animals with two excretory cells was marked for confirmatory testing. Excretory cell counts in confirmatory RNAi experiments, candidate RNAi experiments and experiments with genetic mutants were conducted using 6 cm Petri plates with appropriate media. Animals were first

immobilized by keeping the Petri plates on ice for 30 min. At least 100 animals at the L3-L4 larval stage were scored for each genotype or RNAi experiment unless there was extensive lethality or a growth defect, in which case a lower number or earlier-stage animals, respectively, were scored. A cell was scored as an excretory cell if it was located in the anterior half of the animal and its nucleus had strong GFP expression.

tDHB-GFP fluorescence intensity quantification

The ABplpappap nuclear boundary, cell membrane boundary and the tDHB-GFP fluorescence signal were determined from DIC, mCherry and GFP channels, respectively, of confocal images of RNAi treated *ced-3(lf)* embryos expressing the transgenes *heSi192* and *nIs861*. Mean tDHB-GFP fluorescence intensities inside the nuclear region, entire cell and background were quantified using Fiji software. Mean cytoplasmic tDHB-GFP fluorescence intensity was calculated by the following formula

$$I_{cytoplasm} = \frac{(I_{cell} * cell\ area) - (I_{nucleus} * nucleus\ area)}{cell\ area - nucleus\ area}$$

$I_{cytoplasm}$, I_{cell} and $I_{nucleus}$ denote the mean tDHB fluorescence intensity in the cytoplasm, cell and nucleus, respectively. The ratio of nuclear-to-cytoplasmic tDHB fluorescence intensity in Figure 3H was adjusted for background fluorescence (measured from a random area outside the embryo boundaries), i.e., the background fluorescence intensity was subtracted from both nuclear and cytoplasmic fluorescence intensity values before calculating the ratios.

Calculation of cell size

954 Confocal micrographs were obtained for multiple focal planes starting at the
955 ventral surface and ending at the dorsal surface of the embryo, with each plane
956 separated by a distance of 0.37 μm. The greatest area occupied by a cell in any
957 plane was designated the “maximum area” of a cell.

958 **Cell culture**

959 MDCK and MDCK-Fucci (Streichan et al., 2014) cells were cultured in DMEM
960 supplemented with 10% fetal bovine serum and 1% penicillin/streptomycin in a
961 humidified incubator at 37ºC with 5% CO_2.

962 **Chemicals**

963 2 mM HU (Millipore Sigma, Cat#H8627) was prepared in culture medium prior to
964 each experiment.

965 **Mammalian cell imaging**

966 These assays were performed using 6-well plastic plates. 20,000 MDCK cells
967 were seeded in each well and grown to confluence for 72 h. The day of the
968 experiment, cells were washed twice with PBS and treated with fresh medium or
969 2 mM HU in medium. After equilibration, plates were imaged at 15-min intervals
970 for up to 24 h, using an Evos M7000 imaging system equipped with a humidified
971 onstage incubator (37ºC, 5% CO_2). Several positions per well were imaged in the
972 phase contrast and green and red fluorescence channels available in this
973 system.

974 **Mammalian cell extrusion quantification**

975 In time-lapse phase contrast images, extruding cells are easily identifiable as
976 bright, white, rounded spots emerging from the epithelial plane. We counted the

977 number of cells with these features for each condition using the Cell Counter
978 plugin of Fiji (Schindelin *et al.*, 2012). Extrusions are reported as *number of*
979 *extruding cells/h* for comparison between experiments of different duration.

980 **Mammalian cell cycle phase determination**

981 The Fucci system differentially labels the nuclei of cells in G1 (red) and S/G2/M
982 (green) (Sakaue-Sawano *et al.*, 2008). Images of MDCK-Fucci cells with HU or
983 control treatment were obtained in the phase contrast, red and green
984 fluorescence channels as per Mammalian cell imaging above. For each position,
985 a multi-channel stack was built using Fiji (Schindelin *et al.*, 2012). After
986 identifying an extruded cell in the phase contrast channel, the cell cycle phase
987 was determined using the fluorescence channels.

988 **Mammalian re-seeding experiments**

989 At the end of an imaging experiment, supernatants were collected and
990 centrifuged (1200 rpm, 5 min, room temperature). Pellets were re-suspended in
991 50 µL of PBS, and 10 µL of the suspension was used for cell counting with
992 Trypan blue in a Neubauer chamber, allowing us to simultaneously calculate the
993 number of cells being re-seeded and the fraction of cells that was apoptotic.
994 The remaining cells were seeded with 1 mL of fresh medium in a 24-well plate
995 and grown in the cell culture incubator. Pictures were taken at 2 h and 24 h for
996 cell counting.

997 **Statistical analysis**

998 For calculation of statistical significance for ratios, the ratios were first
999 transformed to logarithm values. Ordinary one-way ANOVA was performed to

determine statistical significance of the ratios with the assumption that logarithm of ratios produced a normal distribution of values. The maximum area of ABplpappap was also assumed to have normal distribution under different RNAi conditions and ordinary one-way ANOVA was used to determine statistical significance. Normal distributions with unequal variances were assumed for rates of extrusion under HU and vehicle treatments, and Welch's two-tailed t-test was performed to determine statistical significance. No assumptions were made about the distributions of the rates of apoptosis under HU and vehicle treatments, and hence the Mann-Whitney test was used to determine statistical significance. No assumptions were made about the distribution of fraction of extruded cells in different phases of the cell cycle after HU and vehicle treatments, and the Kruskal-Wallis test was used to determine statistical significance. Normal distribution was assumed for numbers of cells reseeded in fresh media after pre-treatment in different conditions, and ordinary one-way ANOVA was used to determine statistical significance. All statistical analysis was performed using Prism 7 (GraphPad Software).

References

Andrade, D., and Rosenblatt, J. (2011). Apoptotic regulation of epithelial cellular extrusion. Apoptosis. *16*, 491-501.

Anton, K.A., Kajita, M., Narumi, R., Fujita, Y., and Tada, M. (2018). Src-transformed cells hijack mitosis to extrude from the epithelium. Nat. Commun. *9*, 4695.

Bianchi, V., Zantedeschi, A., and Levis, A.G. (1983). The scintillometric evaluation of DNA repair synthesis can be distorted by changes of thymidine pool radioactivity. Chem. Biol. Interact. *43*,17-31.

Bloom, L., and Horvitz, H.R. (1997). The Caenorhabditis elegans gene *unc-76* and its human homologs define a new gene family involved in axonal outgrowth and fasciculation. Proc. Natl. Acad. Sci. U. S. A. *94*, 3414-3419.

Boeck, M.E., Boyle, T., Bao, Z., Murray, J., Mericle, B., and Waterston, R. (2011). Specific roles for the GATA transcription factors *end-1* and *end-3* during *C. elegans* E-lineage development. Dev. Biol. *358*, 345-355.

Bowman, E.A., Bowman, C.R., Ahn, J.H., and Kelly, W.G. (2013). Phosphorylation of RNA polymerase II is independent of P-TEFb in the *C. elegans* germline. Development. *140*, 3703-3713.

Brauchle, M., Baumer, K., and Gönczy, P. (2003). Differential activation of the DNA replication checkpoint contributes to asynchrony of cell division in *C. elegans* embryos. Curr Biol. *13*, 819-827.

Brenner, S. (1974). The genetics of *Caenorhabditis elegans*. Genetics. *77*, 71-94.

Carroll, T.D., Newton, I.P., Chen, Y., Blow, J.J., and Näthke, I. (2018). Lgr5+ intestinal stem cells reside in an unlicensed G1 phase. J. Cell Biol. *217*, 1667-1685

Chisholm, A.D., and Hardin, J. (2005). Epidermal morphogenesis. WormBook. *1*, 1-22.

Cordes, S., Frank, C.A., and Garriga, G. (2006). The *C. elegans* MELK ortholog PIG-1 regulates cell size asymmetry and daughter cell fate in asymmetric neuroblast divisions. Development *133*, 2747-2756.

De Goeij, J.M., De Kluijver, A., Van Duyl, F.C., Vacelet, J., Wijffels, R.H., De Goeij, A.F.R.M., Cleutjens, J.P.M., and Schutte, B. (2009). Cell kinetics of the marine sponge *Halisarca caerulea* reveal rapid cell turnover and shedding. J. Exp. Biol. *212*, 3892-3900.

Denning, D.P., Hatch, V., and Horvitz, H.R. (2012). Programmed elimination of cells by caspase-independent cell extrusion in *C. elegans*. Nature *488*, 226-230.

Eisenhoffer, G.T., Loftus, P.D., Yoshigi, M., Otsuna, H., Chien, C.B., Morcos, P.A., and Rosenblatt, J. (2012). Crowding induces live cell extrusion to maintain homeostatic cell numbers in epithelia. Nature *484*, 546-549.

Fay, D.S., and Han, M. (2000). Mutations in *cye-1*, a *Caenorhabditis elegans* Cyclin E homolog, reveal coordination between cell-cycle control and vulval development. Development. *127*, 4049-4060.

Fischer, S.E.J., Pan, Q., Breen, P.C., Qi, Y., Shi, Z., Zhang, C., and Ruvkun, G. (2013). Multiple small RNA pathways regulate the silencing of repeated and foreign genes in *C. elegans*. Genes Dev. *27*, 2678-2695.

Fraser, A.G., Kamath, R.S., Zipperlen, P., Martinez-Campos, M., Sohrmann, M., and Ahringer, J. (2000). Functional genomic analysis of *C. elegans* chromosome I by systematic RNA interference. Nature. *408*, 325-330.

Fuchs, Y., and Steller, H. (2011). Programmed cell death in animal development and disease. Cell. *147*, 742-758.

Gaillard, H., García-Muse, T., and Aguilera, A. (2015). Replication stress and cancer. Nat. Rev. Cancer *15*, 276-289.

Grieve, A.G., and Rabouille, C. (2014). Extracellular cleavage of E-cadherin promotes epithelial cell extrusion. J. Cell Sci. *127*, 3331-3346.

Grishok, A., Sinskey, J.L., and Sharp, P.A. (2005). Transcriptional silencing of a transgene by RNAi in the soma of *C. elegans*. Genes Dev. *19*, 683-696.

Gu, Y., and Rosenblatt, J. (2012). New emerging roles for epithelial cell extrusion. Curr. Opin. Cell Biol. *24*, 865-870.

Gu, Y., Shea, J., Slattum, G., Firpo, M.A., Alexander, M., Golubovskaya, V.M., and Rosenblatt, J. (2015). Defective apical extrusion signaling contributes to aggressive tumor hallmarks. Elife. *4*, e04069.

Gudipaty, S.A., and Rosenblatt, J. (2017). Epithelial cell extrusion: Pathways and pathologies. Semin. Cell Dev. Biol. *67*, 132-140.

Gudipaty, S.A., Lindblom, J., Loftus, P.D., Redd, M.J., Edes, K., Davey, C.F., Krishnegowda, V., and Rosenblatt, J. (2017). Mechanical stretch triggers rapid epithelial cell division through Piezo1. Nature. *543*, 118-121.

Günther, J., and Seyfert, H.M. (2018). The first line of defence: insights into mechanisms and relevance of phagocytosis in epithelial cells. Semin. Immunopathol. *40*, 555–565.

Hogan, C., Dupré-Crochet, S., Norman, M., Kajita, M., Zimmermann, C., Pelling, A.E., Piddini, E., Baena-López, L.A., Vincent, J.P., Itoh, Y., Hosoya, H., Pichaud, F., and Fujita, Y. (2009). Characterization of the interface between normal and transformed epithelial cells. Nat. Cell Biol. *11*,460-467.

Hsieh, J., Liu, J., Kostas, S.A., Chang, C., Sternberg, P.W., and Fire, A. (1999). The RING finger/B-box factor TAM-1 and a retinoblastoma-like protein LIN-35 modulate context-dependent gene silencing in *Caenorhabditis elegans*. Genes Dev. *13*, 2958–2970.

Jin, J., Shirogane, T., Xu, L., Nalepa, G., Qin, J., Elledge, S.J., and Harper, J.W. (2003). SCF β-TRCP links Chk1 signaling to degradation of the Cdc25A protein phosphatase. Genes Dev. *17*, 3062-3074.

Jones, M.C., Askari, J.A., Humphries, J.D., and Humphries, M.J. (2018). Cell adhesion is regulated by CDK1 during the cell cycle. J. Cell Biol. *217*, 3203-3218.

Kachur, T.M., Audhya, A., and Pilgrim, D.B. (2008). UNC-45 is required for NMY-2 contractile function in early embryonic polarity establishment and germline cellularization in *C. elegans*. Dev. Biol. *314*, 287-299.

Kajita, M., Hogan, C., Harris, A.R., Dupre-Crochet, S., Itasaki, N., Kawakami, K., Charras, G., Tada, M., and Fujita, Y. (2010). Interaction with surrounding normal epithelial cells influences signalling pathways and behaviour of Src-transformed cells. J. Cell Sci. *123*, 171-180.

Kajita, M., and Fujita, Y. (2015). EDAC: Epithelial defence against cancer - Cell competition between normal and transformed epithelial cells in mammals. J. Biochem. *158*, 15-23.

Kamath, R.S., Fraser, A.G., Dong, Y., Poulin, G., Durbin, R., Gotta, M., Kanapin, A., Le Bot, N., Moreno, S., Sohrmann, M., Welchman, D.P., Zipperlen, P., and Ahringer, J. (2003). Systematic functional analysis of the *Caenorhabditis elegans* genome using RNAi. Nature. *421*, 231-237.

Kipreos, E.T., Gohel, S.P., and Hedgecock, E.M. (2000). The *C. elegans* F-box/WD-repeat protein LIN-23 functions to limit cell division during development. Development. *127*, 5071-5082.

Kocgozlu, L., Saw, T.B., Le, A.P., Yow, I., Shagirov, M., Wong, E., Mège, R.M., Lim, C.T., Toyama, Y., and Ladoux, B. (2016). Epithelial cell packing induces distinct modes of cell extrusions. Curr. Biol. *26*, 2942-2950.

Kocsisova, Z., Kornfeld, K., and Schedl, T. (2018). Cell cycle accumulation of the proliferating cell nuclear antigen PCN-1 transitions from continuous in the adult germline to intermittent in the early embryo of *C. elegans*. BMC Dev. Biol. *18*, 12.

Krawchuk, D., Anani, S., Honma-Yamanaka, N., Polito, S., Shafik, M., and Yamanaka, Y. (2015). Loss of LKB1 leads to impaired epithelial integrity and cell extrusion in the early mouse embryo. J. Cell Sci. *128*, 1011-1022.

Kreutzer, M.A., Richards, J.P., De Silva-Udawatta, M.N., Temenak, J.J., Knoblich, J.A., Lehner, C.F., and Bennett, K.L. (1995). *Caenorhabditis elegans* cyclin A- and B-type genes: A cyclin A multigene family, an ancestral cyclin B3 and differential germline expression. J. Cell Sci. *108*, 2415-2424.

Lee, Y.U., Son, M., Kim, J., Shim, Y.H., and Kawasaki, I. (2016). CDC-25.2, a *C. elegans* ortholog of cdc25, is essential for the progression of intestinal divisions. Cell Cycle. *15*, 654-666.

Leung, C.T., and Brugge, J.S. (2012). Outgrowth of single oncogene-expressing cells from suppressive epithelial environments. Nature. *482*, 410-413.

Mailand, N., Podtelejnikov, A. V., Groth, A., Mann, M., Bartek, J., and Lukas, J. (2002). Regulation of G2/M events by Cdc25A through phosphorylation-dependent modulation of its stability. EMBO J. *21*, 5911-5920.

Marshall, T.W., Lloyd, I.E., Delalande, J.M., Näthke, I., and Rosenblatt, J. (2011). The tumor suppressor adenomatous polyposis coli controls the direction in which a cell extrudes from an epithelium. Mol. Biol. Cell. *22*, 3962-3670.

McMahon, L., Legouis, R., Vonesch, J.L., and Labouesse, M. (2001). Assembly of *C. elegans* apical junctions involves positioning and compaction by LET-413 and protein aggregation by the MAGUK protein DLG-1. J. Cell Sci. *114*, 2265-2277.

Mello, C.C., Kramer, J.M., Stinchcomb, D., and Ambros, V. (1991). Efficient gene transfer in *C. elegans*: extrachromosomal maintenance and integration of transforming sequences. EMBO J. *10*, 3959-3970.

Ohsawa, S., Vaughen, J. and Igaki, T. (2018). Cell extrusion: a stress-responsive force for good or evil in epithelial homeostasis. Dev. Cell *44*, 284-296.

Ossareh-Nazari, B., Katsiarimpa, A., Merlet, J., and Pintard, L. (2016). RNAi-Based suppressor screens reveal genetic interactions between the CRL2LRR-1 E3-ligase and the dna replication machinery in *Caenorhabditis elegans*. G3 Genes, Genomes, Genet. *6*, 3431-3442.

Otto, T., and Sicinski, P. (2017). Cell cycle proteins as promising targets in cancer therapy. Nat. Rev. Cancer. *17*, 93-115.

Rosenblatt, J., Raff, M.C., and Cramer, L.P. (2001). An epithelial cell destined for apoptosis signals its neighbors to extrude it by an actin- and myosin-dependent mechanism. Curr. Biol. *11*, 1847-1857.

Rual, J.F., Ceron, J., Koreth, J., Hao, T., Nicot, A.S., Hirozane-Kishikawa, T., Vandenhaute, J., Orkin, S.H., Hill, D.E., van den Heuvel, S., and Vidal, M. (2004). Toward improving *Caenorhabditis elegans* phenome mapping with an ORFeome-based RNAi library. Genome Res. *14*, 2162-2168.

Sakaue-Sawano, A., Kurokawa, H., Morimura, T., Hanyu, A., Hama, H., Osawa, H., Kashiwagi, S., Fukami, K., Miyata, T., Miyoshi, H., Imamura, T., Ogawa, M., Masai, H., and Miyawaki, A. (2008). Visualizing spatiotemporal dynamics of multicellular cell-cycle progression. Cell. *132*, 487-498.

Saw, T.B., Doostmohammadi, A., Nier, V., Kocgozlu, L., Thampi, S., Toyama, Y., Marcq, P., Lim, C.T., Yeomans, J.M., and Ladoux, B. (2017). Topological defects in epithelia govern cell death and extrusion. Nature. *544*, 212-216.

Schindelin, J., Arganda-Carreras, I., Frise, E., Kaynig, V., Longair, M., Pietzsch, T., Preibisch, S., Rueden, C., Saalfeld, S., Schmid, B., Tinevez, J.Y., White, D.J., Hartenstein, V., Eliceiri, K., Tomancak, P., and Cardona, A. (2012). Fiji: An open-source platform for biological-image analysis. Nat. Methods. *9*, 676-682.

Slattum, G., Gu, Y., Sabbadini, R. and Rosenblatt, J. (2014). Autophagy in oncogenic K-Ras promotes basal extrusion of epithelial cells by degrading S1P. Curr. Biol. *24*, 19–28.

Spencer, S.L., Cappell, S.D., Tsai, F.C., Overton, K.W., Wang, C.L., and Meyer, T. (2013). The proliferation-quiescence decision is controlled by a bifurcation in CDK2 activity at mitotic exit. Cell *155*, 369-383.

Stevens, H., Williams, A.B., and Michael, W.M. (2016). Cell-type specific responses to DNA replication stress in early *C. elegans* embryos. PLoS One *11*, e0164601.

Streichan, S.J., Hoerner, C.R., Schneidt, T., Holzer, D., and Hufnagel, L. (2014). Spatial constraints control cell proliferation in tissues. Proc. Natl. Acad. Sci. *111*, 5586-5591.

Sulston, J.E., Schierenberg, E., White, J.G., and Thomson, J.N. (1983). The embryonic cell lineage of the nematode *Caenorhabditis elegans*. Dev Biol. *100*, 64-119.

Teuliere, J., Cordes, S., Singhvi, A., Talavera, K., and Garriga, G. (2014). Asymmetric neuroblast divisions producing apoptotic cells require the cytohesin GRP-1 in *Caenorhabditis elegans*. Genetics. *198*, 229-247.

Timson, J. (1975). Hydroxyurea. Mutat. Res. *32*, 115-132.

van den Heuvel, S. (2005). Cell cycle regulation. WormBook, ed. The *C. elegans* Research Community WormBook, WormBook.

van Rijnberk, L.M., van der Horst, S.E., van den Heuvel, S. and Ruijtenberg, S. (2017). A dual transcriptional reporter and CDK-activity sensor marks cell cycle entry and progression in *C. elegans*. PLoS One *12*, e0171600.

Wallenfang, M.R., and Seydoux, G. (2002). *cdk-7* is required for mRNA transcription and cell cycle progression in *Caenorhabditis elegans* embryos. Proc. Natl. Acad. Sci. U. S. A. *99*, 5527-5532.

Wernike, D., Chen, Y., Mastronardi, K., Makil, N., and Piekny, A. (2016). Mechanical forces drive neuroblast morphogenesis and are required for epidermal closure. Dev. Biol. *412*, 261-277.

Wu, S. K., Gomez, G. A., Michael, M., Verma, S., Cox, H. L., Lefevre, J. G., Parton, R. G., Hamilton, N. A., Neufeld, Z. and Yap, A. S. (2014). Cortical F-actin stabilization generates apical-lateral patterns of junctional contractility that integrate cells into epithelia. Nat. Cell Biol. *16*, 167–178.

Xiao, Z., Chen, Z., Gunasekera, A.H., Sowin, T.J., Rosenberg, S.H., Fesik, S., and Zhang, H. (2003). Chk1 mediates S and G2 arrests through Cdc25A degradation in response to DNA-damaging agents. J. Biol. Chem. 278, 21767-21773.

Yazinski, S.A., and Zou, L. (2016). Functions, regulation, and therapeutic implications of the ATR checkpoint pathway. Annu. Rev. Genet. *50*, 155-173.

Yeong, F.M. (2004). Anaphase-promoting complex in *Caenorhabditis elegans*. Mol. Cell. Biol. *24*, 2215-2225.

Zeman, M.K., and Cimprich, K.A. (2014). Causes and consequences of replication stress. Nat. Cell Biol. *16*, 2-9.

Zerjatke, T., Gak, I.A., Kirova, D., Fuhrmann, M., Daniel, K., Gonciarz, M., Müller, D., Glauche, I., and Mansfeld, J. (2017). Quantitative cell cycle analysis based on an endogenous all-in-one reporter for cell tracking and classification. Cell Rep. *19*, 1953-1966.

Ziel, J.W., Hagedorn, E.J., Audhya, A., and Sherwood, D.R. (2009). UNC-6 (netrin) orients the invasive membrane of the anchor cell in *C. elegans.* Nat. Cell Biol. *11*, 183-189.